On the relationship between thermodynamic disequilibrium ratio and flux control of metabolic pathways

by

Frederik Christoffel Rust

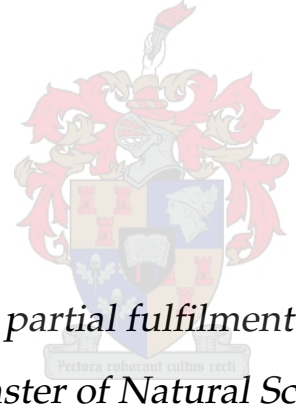

Thesis presented in partial fulfilment of the requirements for the degree of Master of Natural Science (Biochemistry) in the Faculty of Natural Science at Stellenbosch University

Supervisor: Prof. J. Snoep

Co-supervisor: Dr. D. van Niekerk

December 2021

Declaration

By submitting this thesis electronically, I declare that the entirety of the work contained therein is my own, original work, that I am the sole author thereof (save to the extent explicitly otherwise stated), that reproduction and publication thereof by Stellenbosch University will not infringe any third party rights and that I have not previously in its entirety or in part submitted it for obtaining any qualification.

Date: 2021/08/14 .....

Abstract

This study presents a methodology to determine and compare flux control coefficients, as defined in the metabolic control analysis framework, with disequilibrium ratios of reactions in metabolic pathways at steady-state. This is accomplished in the form of an automated computational algorithm written in Wolfram Mathematica that 1) retrieves models from online repositories via an Application Programming Interface (API), 2) calculates flux control coefficients, and 3) determines disequilibrium ratios using the symbolic forms of reaction rate equations.

The analysis was started with 778 models obtained from the JWS Online and Biomodels databases, of which 164 remained, leading to a total of 1234 reactions, after testing for suitability of the models and reactions for the analysis. Probability density plots of the flux control coefficients against the disequilibrium ratios showed clearly that the vast majority of reactions with a flux control coefficient, on their own flux, greater than 0.25 had a disequilibrium ratio smaller than 0.2. Furthermore the plot shows that the majority of reactions have flux control coefficients smaller than 0.2, and that reactions tend to have either high (>0.6) or low (<0.3) disequilibrium ratios, which was strongly influenced by presence or absence of product sensitivity in the denominator of the rate equations.

Samevatting

Hierdie studie bied ’n metodologie aan om fluksiekontrole-koëffisiënte, soos gedefinieer in die metaboliese kontrole analise raamwerk,te bepaal en te vergelyk met disekwilibriumverhoudings van reaksies in metaboliese padweë by ’n bestendige toestand. Dit word bewerkstellig in die vorm van ’n outomatiese berekeningsalgoritme geskryf in Wolfram Mathematica wat 1) modelle van aanlynbewaarplekke via ’n programmeringskoppelvlak (API) haal, 2) fluksiekontrolekoëffisiënte bereken, en 3) disekwilibriumverhoudings bepaal deur gebruik te maak van die simboliese vorms van reaksiesnelheidsvergelykings.

Die ontleding is begin met 778 modelle verkry vanaf die JWS Online en Biomodels databasisse, waarvan 164 oorgebly het, wat gelei het tot ’n totaal van 1234 reaksies, na toetsing vir geskiktheid van die modelle en reaksies vir die analise. Waarskynlikheidsdigtheid-grafieke van die fluskiekontrolekoëffisiënte teenoor die disekwilibriumverhoudings het duidelik getoon dat die oorgrote meerderheid reaksies met ’n fluskiekontrolekoëffisiënt groter as 0.25 ’n disekwilibriumverhouding kleiner as 0.2 gehad het. Verder toon die grafiek dat die meerderheid reaksies fluskiekontrolekoëffisiënte kleiner as 0.2 het, en dat reaksies geneig is om óf hoë (>0.6) óf lae (<0.3) disekwilibriumverhoudings te hê, wat sterk beïnvloed is deur die teenwoordigheid of afwesigheid van produksensitiwiteit in die noemer van die snelheidsvergelykings.

Acknowledgements

I would like to express my sincere gratitude to the following people and organisations:

To my Supervisor Prof. J. Snoep, for a guiding hand. For keeping me grounded to the bigger picture and for keeping faith.

To my Co-Supervisor Dr. D. van Niekerk, for hours of stimulating discussions.

The JJJ Lab and co-workers, for putting up with the learning curve associated with the occasional accidental simulation interruptions.

My Family, as they have been with me every step of the way .

Contents

List of Figures

Glossary

API Application Program Interface; Is a link between various applications or programs described by a clearly defined specification for information transfer. viii, 25, 26

MCA Metabolic Control Analysis; A subset of sensitivity analysis, a mathematical framework used to quantify sensitivity and control in metabolic, signaling and genetic pathways. 2, 12, 13, 16

MF Matrix Format; An internal model format used by JWS Online metabolic network calculators. (*i.e.* Teusink-Glycolysis.mf). 28, 30

REST Representational State Transfer; A subset of API allowing for a stateless communication protocol. 25, 26, 30

SBML Systems Biology Mark-up Language; A standardized description language used to transcribe biological model data. www.sbml.org. 2, 28, 29

steady-state A state where the rate of formation of metabolites equal the rates of degradation, leaving the system in a dynamic equilibrium. 12–14, 17, 32

Chapter 1

Introduction

Large scale genomics and metabolic studies are generating more data than can be managed by the human mind alone [1–3]. Increasingly, this knowledge is stored by means of mathematical models generated from observed biological phenomena. These models are typically geared towards not only describing but also understanding and ultimately predicting the time evolution of perturbations on various collective or specific parts of biological systems.

The modeling process is the synthesis of knowledge, from experimentally repeatable observations to parameterized mathematical equations. The derivation and interrogation of such models have been of central interest to various fields of biological research. Two distinct stages are involved in the modeling process; construction and validation. These two stages form a continuous development cycle, adapting and improving the model, until the desired degree of accuracy and validity is achieved.

The construction of a biochemical model follows from the initial identification of the system, to the description of its time dependant variables in terms of system properties such as stoichiometries, interaction mechanisms, equilibrium

constants, reaction rates and enzyme binding constants. The validation of the model involves testing of a model's ability to accurately predict experimental results which has not been used in its construction[4].

For future use, a model can be formatted in the systems biology markup language (SBML) and stored in on-line model repositories such as BioModels and JWSOnline. Models in repositories can, inter alia, be interrogated and analyzed by computational methods to test a hypothesis. One such hypothesis will be analysed in this thesis, namely that a relationship exists between the flux control coefficient and the disequilibrium ratio of an enzyme catalyzed reaction.

In addition to the fundamental knowledge aspect, this question is relevant for accelerated methods of detecting enzymatic drug targets. Further applications can be found in the biotech industries, where faster determination of key enzyme levels can lead to savings and gains in production efficiencies.

In this thesis, we aim to test whether a relationship exists between the flux control coefficient and disequilibrium ratio of reactions in mathematical models, not only for a single network, but across many hundreds of networks, available in model databases, using internet communication protocols and scripting software. A method for automated disequilibrium calculations was developed and control calculations were done by means of metabolic control analysis (MCA). To meet this aim, the following objectives were defined and the structure of the thesis follows this layout:

1. Literature review to evaluate
    - Current approaches towards automated disequilibrium and flux control coefficient determinations.

- Current views on relationships between disequilibrium ratio and flux control coefficient.
- Existing work on MCA.
- Current frameworks on data mining.
- Mathematica documentation of functions involved.
- Current web development practices in communications protocols.

2. Retrieve of data from online repositories.
   - Retrieve model repository API endpoint information.
   - Construct function utilising API endpoint.
   - Construct functions to identify and log errors in model retrieval.
   - Manage model data as to maintain trace-ability within a parallel computing environment.
3. Calculate flux control coefficient and disequilibrium ratios.
   - Filter models based on defined criteria for calculations.
   - Calculate flux control coefficients.
   - Determine reaction reversibility.
   - Identify substrates and products for each reaction.
   - Calculate mass action ratios (Γ).
   - Symbolically identify and numerically calculate K_{eq}
   - Calculate disequilibrium ratios (ρ).
4. Visualise and interpret results.
   - Normalize data by taking the reciprocal of disequilibrium ratios larger than one.

- Visualise probability density function on two dimensional graph.
- Train machine learning predictor on data and visualize probability density functions of different control coefficients.
- Compare percentages of reactions for various disequilibrium and flux control coefficient ranges.
- Relate computational prediction, percentage calculations and visual observations to one another.

Chapter 2

Literature Review and Background

This chapter aims to bring together the current literature and aspects of thermodynamics, metabolic control analysis, and biochemical modelling. This is done to lay the foundation for understanding a possible relationship between flux control coefficients and the thermodynamic disequilibrium ratios.

The following are some theoretical fundamentals to thermodynamics. This will be followed by an overview of biochemical modeling and metabolic control analysis.

2.1 Thermodynamics

From the first law of thermodynamics energy is known to be indestructible and finite. This brings about a cyclic conservation of energy in a closed system, whereby transitions from higher to lower energy states are, in principle, reversible. In reality such a reversal will not occur spontaneously, e.g. a pile of ash will not spontaneously return to a stack of logs. This is addressed by the second law of thermodynamics which introduces entropy (S) with units of J/K. En-

tropy frames the net direction of a reaction: reactions leading to a spread of the system across more states (an increased disorderedness) have positive entropy changes and will occur spontaneously. The third law of thermodynamics then apply these changes in entropy to an absolute scale, with formulations ranging from quantum mechanical to classical interpretations.

Energy/matter exists in accordance with these laws of thermodynamics, in a continual flux towards highest entropy. Within this context, energy flow predictably follows along paths of least resistance. As such, regulatory strategies of living systems have had to develop and adapt to maintain conditions that are favourable for sustaining life within thermodynamic constraints. Life has at times been described as an intermediate stability, altering through ever changing states [5]. This leaves the probability that regulatory strategies of living systems have developed in such a way as to be reflective of the underlying thermodynamic properties of the individual components involved. [6].

Entropy (S), as the main driving force in thermodynamics, is said to give rise to the arrow of time [7]. In chemistry, S can be described in the degrees of freedom of interacting molecules. The formation of new bonds brings about a decrease in degrees of freedom and as such a decrease in entropy of the molecules but an increase in entropy of the environment due to e.g. heat release. The system and environment undergoes change from one state towards a statistically more probable one [8]. In biochemical systems these states are further influenced by constraints on compartmental environments such as vessels, cells and organelles [4, 9, 10]. Irrespective of constraints however, the underlying laws of thermodynamics hold and a change in state is invariably bound to a change in energy. Such a change can relate to a decrease in S of the system itself, but is ultimately leading to an increase in total S (system + environment).

In biochemical systems, typically functioning at fixed pressure and volumes, entropy is incorporated by means of the Gibbs free energy change (ΔG). ΔG is defined as the overall change in energy of a system, accounting for the change in internal energy (ΔH) and entropy (ΔS) [11, 12]:

$$\Delta G = \Delta H - T\Delta S \tag{2.1}$$

ΔG also yields insight into the direction of a reaction based on the current thermodynamic state. With a natural tendency towards a decrease in Gibbs free energy, reactions with a negative ΔG will proceed spontaneously. These are more commonly referred to as exergonic reactions. A positive ΔG in turn indicates a reaction requiring the addition of energy to proceed, also termed an endergonic reaction. Note however that ΔG does not give information on the rate of a reaction, but rather on its energetic favourability. One can define the Gibbs free energy change of a reaction in terms of direction and distance from equilibrium by taking account of the mass-action ratio $\Gamma = {}^{[\text{products}]}/_{[\text{substrates}]}$ at the current state and the reaction's equilibrium constant:

$$\Delta G = RT \ln \frac{\Gamma}{K_{eq}} = \Delta G^0 + RT \ln \Gamma \tag{2.2}$$

with R being the ideal gas constant and T the temperature in Kelvin. The standard (biochemical) Gibbs free energy (ΔG^0) is defined by the standard state, in which a constant pressure of 1 atm a temperature of 298 K a concentration of $1M$ for all species and a pH of 7 is maintained, i.e. if $\Gamma = 1$ eq. 2.2 becomes $\Delta G = \Delta G^0$.

At equilibrium, $\Delta G = 0$, and eq. 2.2 becomes $\Delta G^0 = -RT \ln K_{eq}$. For a reaction substrates $\rightleftharpoons$ products, the equilibrium constant K_{eq} can be defined as

$$K_{eq} = \frac{[\text{products}]_{eq}}{[\text{substrates}]_{eq}} \tag{2.3}$$

From the above, it is clear that the equilibrium state and the current metabolite state relate to the change in Gibbs free energy of a reaction. However, the Gibbs free energy change as defined above does not give information about individual species contributions towards the energy change as a whole.

Since biochemical systems constitute multi-molecular solutions, the general Gibbs free energy change can be adapted to more fully describe individual species partial contributions towards the full Gibbs free energy change. This partial change per species unit (i) is termed the chemical potential (μ). ΔH in equation 2.1 describes the change to internal energy, as being equal to the total internal species energy U plus the product of the pressure P and volume V.

$$H = U + PV \tag{2.4}$$

U can be rewritten in terms of the sum of chemical potentials μ of species N involved in the exchange of the number of units i, such that

$$H = \sum_{i=1}^{n} \mu_i N_i + PV \tag{2.5}$$

Substituting H back into equation 2.1, the Gibbs free energy change for the system, at constant pressure and volume can now be defined in terms of individual species contributions:

$$\Delta G = \sum_{i=1}^{n} \mu_i N_i - T\Delta S \tag{2.6}$$

Through the chemical potentials and Gibbs free energy changes, a description of the reaction direction as well as distance from equilibrium is quantifiable. However, the Gibbs free energy change does not yield information on the regulatory mechanisms or specific rates in reaction networks. These are tasks handled by the construction of biochemical models using reaction rate equations.

2.2 Biochemical Modeling

Mechanistic models of metabolic pathways encode biochemical knowledge of the system in mathematical formalism. Rate equations for the individual processes are an important part of the mathematical structure upon which a model is built as they link the variables in a model into a functioning metabolic network.

2.2.1 Rate equations

Rate equations are constructed from rate laws with parameters typically determined from experimental observations. This serves as an initial step towards defining the structure and overall regulatory properties of the system [4, 13, 14]. A fundamental rate law, the law of mass action was derived from thermodynamic principles by van't Hoff [15–17]. The law of mass action has since been used as the basis for more generic rate equations. An example of such an equation describes the rate (v_a) of the reaction $a + b \longrightarrow c$ as

$$v_a = k[a]^{\alpha}[b]^{\beta} \tag{2.7}$$

where the rate of the reaction (v_a) is affected by metabolite concentrations ($[a]$, $[b]$), reaction order (α, β) and rate constant (k). Reaction orders quantify a reac-

tion's sensitivity to changes in metabolite concentrations. The rate constant can be defined by the Arrhenius equation:

$$k = Ae^{-\frac{E_A}{RT}} \tag{2.8}$$

and is dependent upon temperature (T), activation energy (E_A), the gas constant (R) and a spatial frequency factor (A) [18, 19].

Since reactions do not only proceed in one direction, an expansion on the example above is necessary to consider the equilibrium state. By defining the reaction reversibly such that $a + b \rightleftharpoons c$ the need for a net rate of change (v_{net}) becomes apparent. The reaction in the forward direction, defined as the consumption of a and b, is

$$v_{forward} = k_{forward}[a]^{\alpha}[b]^{\beta} \tag{2.9}$$

and the reverse reaction leading to the production of a and b is

$$v_{reverse} = k_{reverse}[c]^{\gamma} \tag{2.10}$$

The net reaction rate is the difference:

$$v_{net} = v_{forward} - v_{reverse} \tag{2.11}$$

One can substitute equations 2.9 and 2.10 into equation 2.11 yielding

$$v_{net} = k_{forward}[a]^{\alpha}[b]^{\beta} - k_{reverse}[c]^{\gamma} \tag{2.12}$$

and at equilibrium

$$v_{net} = 0 \tag{2.13}$$

so that

$$v_{forward} = v_{reverse} \tag{2.14}$$

. At equilibrium the mass action ratio (Γ) and equilibrium constant (K_{eq}) are equal. Deviations from equilibrium can be quantified by means of the disequilibrium ratio (ρ) so that at equilibrium

$$\rho = \frac{\Gamma}{K_{eq}} = 1 \tag{2.15}$$

The Haldane relationship relates the equilibrium condition to both the thermodynamic and kinetic properties by way of the mass action ratio and rate constants, such that

$$\frac{[c]_{eq}}{[a]_{eq}[b]_{eq}} = K_{eq} = \frac{k_{forward}}{k_{reverse}} \tag{2.16}$$

In the context of enzyme catalyzed reactions, the hyperbolic Michaelis-Menten equation is often used to describe the rate of a reaction. In the simple case of a single substrate S and single product P reversible reaction the rate can be written as:

$$v_i = \frac{V_f \frac{[S]}{K_s} - V_r \frac{[P]}{K_p}}{1 + \frac{[S]}{K_s} + \frac{[P]}{K_p}} \tag{2.17}$$

with V_f and V_r being the maximum rates at which the enzyme catalyzed reaction occurs (full saturation of catalytic sites) in the forward and reverse directions. K_s and K_p in turn are the dissociation constants of substrate or product. The derivations for equilibrium, mass action ratio and the Haldane relation shown above, extends straightforwardly to enzyme catalyzed reactions also, leading to the Haldane relation in the form

$$K_{eq} = \frac{V_f \cdot K_p}{V_r \cdot K_s} \tag{2.18}$$

Rate laws and equations such as the ones described above, have formed the basis of analysing experimental observations within a mathematical framework (with modifications in the case of enzyme catalyzed reactions). Biochemical models are constructed by linking together many of these rate equations in an ODE structure. This structure resembles a metabolic network of production and consumption rates leading to changes in metabolic concentrations [3, 20, 21].

2.3 Metabolic Control Analysis (MCA)

Advances in biological understanding in the form of mathematical frameworks that incorporate both structural and kinetic information of systems have enabled analysis methods such as MCA. MCA is a type of sensitivity analysis applied to metabolic systems and systematically quantifies effects upon system properties as brought about by alterations in local components. Effects of such alterations, also known as perturbations, are typically investigated at steady-state. This state defines a dynamic equilibrium, whereby the boundary metabolites, also known as pools and sinks or external metabolites, are held constant (buffered). MCA has also been adapted to the investigation of systems at dynamic non-steady-states [22]. Upon perturbation the system settles to a new steady-state. Depending upon the type of perturbation study, the flux control-, concentration control- and elasticity coefficients are three sensitivity coefficients that can be determined [23, 24].

2.3.1 Control coefficients and elasticities

The flux control coefficient (C_i^J), quantifies the percent change in flux, brought about by a one percent change in enzyme activity (v_i):

$$C_i^J = \frac{\delta J}{J} / \frac{\delta v_i}{v_i} \tag{2.19}$$

The concentration control coefficient (C_i^S), describes the effect on steady-state metabolite (S), given a change in enzyme activity (v_i), note that in the current study J will refer to the flux through reaction i:

$$C_i^S = \frac{\delta S}{S} / \frac{\delta v_i}{v_i} \tag{2.20}$$

Elasticity relates a relative change in a local parameter to the corresponding relative local change in a reaction rate. For example, the effect of temperature, fixed metabolite or inhibitor concentrations and pH. The elasticity coefficient can be written as:

$$\varepsilon_P^{v_i} = \frac{\delta v_i}{v_i} / \frac{\delta P}{P} \tag{2.21}$$

Whilst the first two, respectively termed the flux control and concentration control coefficients, relate activity changes to global steady-state effects, the elasticity coefficient relates local perturbations to local activity effects.

From these control and elasticity coefficients two relationships, the connectivity and control theorems, were derived in the 1970's and 1980's initially by Heinrich, Rapoport, Kascer and Burns and extended by a large group of researchers [23, 25–28]. This framework is reviewed in full by Fell [4]. These theorems relate the coefficients to one another and place constraints within which a more systemic analysis can be performed.

The implication and applications of MCA have been far reaching, bringing about new insights and developments to the domains of Biochemistry, Medicine,

Biotechnology, Physiology, Pharmaceuticals, Genetics, Botany, Immunology and Agriculture [14, 29–35].

2.3.2 Summation and Connectivity Theorems

The summation theorem as described by Kacser and Burns, Rapoport et al. [23, 27] sets constraints on the above mentioned coefficients, such that

$$\sum_i C^J_{v_i} = 1 \tag{2.22}$$

$$\sum_i C^S_{v_i} = 0 \tag{2.23}$$

Equations 2.22 and 2.23 describe the distribution of flux and concentration control throughout the system, with each reaction potentially contributing towards the whole of control in the pathway.

The easiest way to conceive the summation theorem is to consider a system at steady-state, and then make an equal change to all the reactions. When all reactions are changed equally, none of the metabolite concentrations will change but the flux will change proportionally to the perturbation.

Connectivity theorems in turn define the link between local enzyme kinetic properties and global pathway variables. The first is known as the flux connectivity theorem and can be used to illustrate how flux control is inversely proportional to elasticity:

$$\sum_{v_i} C^J_{v_i} \epsilon^{v_i}_S = 0 \tag{2.24}$$

For instance, for a two enzyme system with intermediate x, the following holds:

$$C^J_{v_1}\epsilon^{v_1}_x = -C^J_{v_2}\epsilon^{v_2}_x \tag{2.25}$$

and

$$C^J_{v_1}/C^J_{v_2} = -\epsilon^{v_2}_x/\epsilon^{v_1}_x \tag{2.26}$$

The second, known as the concentration connectivity theorem, involves the summation property of the products of concentration control and elasticity coefficients. This theorem is subdivided into two equations with the first considering reactions with species applicable to elasticity considerations (S_m) differing from ones applicable to concentration control coefficients (S_n). The second considers these elasticity and concentration control coefficients for the same species[23, 36]:

$$\sum_{v_i} C^{S_n}_{v_i}\epsilon^{v_i}_{S_m} = 0 \quad \text{for} \quad m \neq n \tag{2.27}$$

$$\sum_{v_i} C^{S_n}_{v_i}\epsilon^{v_i}_{S_m} = -1 \quad \text{for} \quad m = n \tag{2.28}$$

Using the summation and connectivity theorems, control coefficients can be expressed in terms of local properties (the elasticity coefficients). In a system of two reactions with common intermediate x:

$$C^x_{v_1} = \frac{1}{\epsilon^{v_1}_x - \epsilon^{v_2}_x} \tag{2.29}$$

$$C_{v_2}^{x} = \frac{-1}{\epsilon_x^{v_2} - \epsilon_x^{v_1}} \tag{2.30}$$

The two flux control coefficients of the simple two enzyme pathway can be expressed in terms of elasticities as follows:

$$C_{v_1}^{J} = \frac{\epsilon_x^{v_2}}{\epsilon_x^{v_2} - \epsilon_x^{v_1}} \tag{2.31}$$

$$C_{v_2}^{J} = \frac{-\epsilon_x^{v_1}}{\epsilon_x^{v_2} - \epsilon_x^{v_1}} \tag{2.32}$$

These relationships have been further extended using symbolic matrix algebra methods [25, 37–39]. With these tools, investigations into and the understanding of regulation in biological networks can occur on the level of the system. Many research activities have been geared towards discerning a so-called rate-limiting step in a metabolic pathway, adopted from chemistry where the overall reaction rate is approximately determined by the slowest rate in the reaction chain. This concept leads to a somewhat oversimplified view of regulatory strategies in metabolic networks. MCA and its associated theorems, quantifies the finite-contribution of each reaction towards the distributed control over the system as a whole.

2.3.3 Linear Algebra Methods in MCA

In this section a short overview of the relevant formalism is provided. For a more complete derivation, refer to [39].

The stoichiometric matrix (N) is defined by placing the stoichiometric dependency of all reactions M on species S in rows such that an m-by-s matrix is

formed. The reduction of this N matrix to row echelon form by Gaussian elimination leads to the reduced matrix N_R containing the stoichiometry of the independent species of the system. It is related to the original N matrix via a link matrix L, defined such that $N = LN_R$.

The matix of elasticity coefficients $\bar{\mathcal{E}}$ is determined by taking partial derivatives of each reaction rate with respect to steady state metabolite concentrations. This notation stems from the article by [39] whereby a bar on $\bar{\mathcal{E}}$ denotes non-scaled elasticities. Scaling can be done by taking the normalising change to the reference state (see eq. 2.21), producing dimensionless elasticities $\mathcal{E}$.

The Jacobian matrix M, defined as the first-order partial derivative of a vector function, can be used to quantify the behaviour around a steady-state. The Jacobian matrix can be calculated by multiplying the reduced stoichiometry matrix N_R, non-scaled elasticities $\bar{\mathcal{E}}$ and link matrix L such that

$$M = N_R \bar{\mathcal{E}} L \tag{2.33}$$

The Jacobian matrix is used in calculating concentration control coefficients. The concentration control coefficient, eq. 2.20, indicates the relative changes to metabolite concentrations S brought about by rate perturbations v. From the matrix formalism the concentration control coefficients $\bar{C}^s$ can be calculated from the link matrix L the Jacobian matrix M and the reduced stoichometry matrix N_R such that

$$\bar{C}^s = -LM^{-1}N_R \tag{2.34}$$

From this, flux control coefficients $\bar{C}^J$ are calculated as

$$\bar{C}^J = \bar{\mathcal{E}}_s \bar{C}^s + I_m \tag{2.35}$$

with I_m the identity matrix I of size m [39].

2.4 Thermodynamics and flux control

Via a separation of the kinetic and thermodynamic factors in enzyme rate equations we can analyze the extreme conditions of either complete saturation of enzymes with intermediates or the case where the intermediates have much lower concentrations than their K_m values. For the latter case the control coefficients of an enzyme can be expressed in terms of thermodynamic properties as is illustrated for linear pathways by Kacser et al. [37], Fell [4] and Sauro [40].

As an example, consider a network consisting of a connection of two reactions via a common intermediate; reaction 1: $S \rightarrow X$, reaction 2: $X \rightarrow P$. Where the enzyme activity for a uni-uni reaction ($S \longrightarrow X$) is described by a generic rate equation:

$$v = V_m \cdot \frac{s/K_s}{1 + s/K_s + x/K_{1x}} \cdot (1 - \Gamma/K_{eq}) \tag{2.36}$$

Splitting up a rate equation into thermodynamic and kinetics parts can be done for enzyme kinetic rate equations in general Rohwer and Hofmeyr [41]. Using equation 2.21 one can express the elasticities ϵ_x^v in terms of enzyme kinetic parameters by taking the partial derivative of the rate equation with respect to x, and normalizing by the steady state values of x and v

$$\epsilon_x^{v_i} = \underbrace{\frac{-1}{1-\rho_1}}_{\text{thermodynamic}} + \underbrace{\frac{1}{1+x/K_x \cdot K_s/(s+K_s)}}_{\text{enzyme kinetic}} \tag{2.37}$$

where Γ/K_{eq} has been replaced by ρ_1. In equation 2.36, the kinetic terms leads to the typical hyperbolic curve with a proportional increase in enzyme activity at $s < K_s$ values and the activity asymptotically reaching (V_{max}) at $s >> K_s$ values. These extremes can be used to make a simplification to equation 2.37: if the intermediate concentrations are much lower than the K_m values:

$$\lim_{K_x \to \infty} \epsilon_x^{v_1} = \frac{1}{1-1/\rho_1} \tag{2.38}$$

Similarly for the elasticity of reaction 2 with respect to x:

$$\epsilon_x^{v_2} = \frac{1}{-1+1/\rho_2} + \frac{1}{1+x/K_x \cdot K_p/(p+K_p)} \tag{2.39}$$

with:

$$\lim_{K_x \to \infty} \epsilon_x^{v_2} = \frac{1}{1-\rho_2} \tag{2.40}$$

By substituting the respective expressions for the elasticities in equations 2.31 and 2.32 we obtain

$$\lim_{K_x \to \infty} C_{v_1}^J = \frac{1-\rho_1}{1-\rho} \tag{2.41}$$

$$\lim_{K_x \to \infty} C_{v_2}^J = \frac{\rho_1(1-\rho_2)}{1-\rho} \tag{2.42}$$

with ρ defined as the product of the disequilibrium ratios of the respective steps in the pathway, i.e. $\rho_1 \cdot \rho_2$, being a measure for the degree to which the pathway is away from equilibrium. The equation can be extended for longer unbroken linear pathways with single flux [40]:

$$\lim_{K_x \to \infty} C^J_{v_k} = \frac{\prod_{i=1}^{k-1} \rho_i (1 - \rho_k)}{1 - \rho} \tag{2.43}$$

Equation 2.43 can be used to calculate a reaction's control coefficients on the basis of the displacement from equilibrium of the steps "before" the reaction. Note that ρ is a pathway property and can be calculated without detailed knowledge of all the steps.

From the above it is clear that under certain conditions (very low or very high metabolite concentrations) and in certain networks (e.g. a linear pathway) a relation between the disequilibrium ratio (thermodynamics) and the flux control of a reaction exists, although not necessarily simple.

In this thesis we re-examined a long standing discussion that started in the 1960s, (and was kind of put to rest with the development of metabolic control analysis in the 1970-1980s), whether so called rate-limiting steps can be identified as those reactions that are far away from equilibrium. The historical context, with references to the original literature, is given in Fell's excellent book [4], and the final conclusion was that reactions close to equilibrium tend to have less control than enzymes far away from equilibrium, but these are trends, and to be sure one needs to use flux control coefficients to define the flux control distributions over a network. However, since it is much easier (although far from trivial) to measure the disequilibrium ratio of a reaction than it is to determine a flux control coefficient, it would be interesting to test for a large number of reac-

tions how good a correlation is observed between the two entities. So whereas we do not want to re-open the discussion, which in our opinion is settled, we were interested in testing the original proposal for a large set of reactions. To our knowledge such a systematic test has not been made for the large number of models available in model databases, and that is what we set out to do in this study.

Chapter 3

Methodology

This chapter describes the steps that were followed towards an automated determination of flux control coefficients and disequilibrium ratios. These calculations were performed on metabolic models at steady state. A list of all the models included in the final results is available in Appendix A.1. The development of a first generation database mining-system as defined by Imielinski and Mannila, Radivojac et al. and Uppalaiah et al. served as the outline for the process of data-handling and followed these four objectives [42–44].

1. Data processing
2. Transformation
3. Analysis
4. Visualization

Towards this goal, a description of the installation of an isolated working environment in silico occupies the first section of this Chapter. The four objectives as set out above then define the individual components of the algorithm as outlined in Figure 3.1.

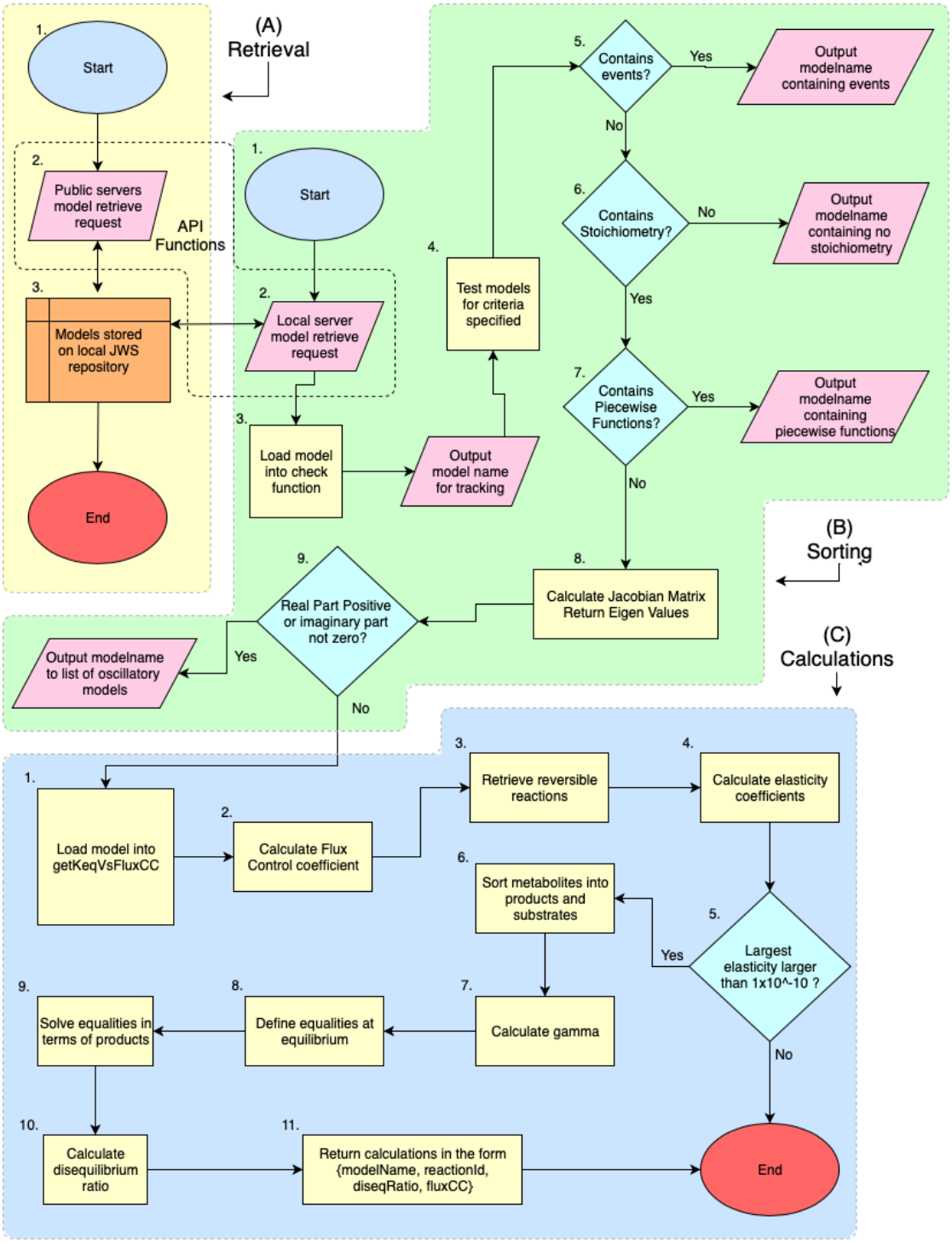

Figure 3.1: Overview diagram of the complete workflow during run-time. With reference to the data-handling objectives in Chapter 3, retrieval (A) and sorting (B) encompasses the data processing portion, whilst calculations (C) refer to the data transformation process.

3.1 Setting up the working environment

The working environment was constructed in two parts; consisting of a data management and scripting components. For the data management aspect, a local instance of JWS Online was used for the retrieval, storage and translation of model information whilst Wolfram Mathematica v12 served as the scripting environment. Mathematica was chosen as it is both the most prominent platform utilised in our research group as well as forming the back-end of model simulation in JWS Online. Mathematica is furthermore specifically well suited towards direct symbolic equation handling, which will be discussed later in this Chapter.

The JWS Online server instance was hosted within the Docker platform. For a more complete JWS Online docker installation and reference guide, please refer to the documentation available at `https://jws-docs.readthedocs.io`.

3.1.1 JWS Online and Docker installation

A locally hosted JWS Online server was set-up to achieve isolation from active production environments as to not inundate public JWS Online servers with repetitive model upload, download, query and conversion operations. This proved especially useful considering the repetitive nature associated with a development and testing cycle for thousands of models. An added benefit was an increase in overall efficiency when considering the time taken to handle the entire data-set. This was primarily due to internet connection speed and connection reliability affecting the retrieval of models from public servers. Overhead communication rates, between Mathematica and the local server instance, was limited only by processor transfer rates.

Docker is an open source platform, with the advantage of being operating sys-

tem agnostic built in by definition. As such a Docker environment is self contained and easily reproducible in any operating system. The Docker host application was downloaded and installed for the operating system of choice (MacOS) as instructed by the docker documentation available at http://docker-sean.readthedocs.io. The JWS Online Docker compose script (http://jws-docs.readthedocs.io/10_docker.html) documents the process of setting up JWS Online with docker. Further general information on Docker installation is available at https://docs.docker.com/compose/compose-file. After setup, a successful installation and startup can be confirmed by visiting the localhost or loop-back IP address (127.0.0.1), in the web browser of choice, and being greeted by a local JWS Online instance homepage.

With JWS Online active as the model handling part of the working environment, a communication method from the scripting language, Mathematica, is needed. The communications method native to JWS Online is in the form of a representational state transfer (REST) application program interface (API). As this is the basis of data transfer, the following section will provide a brief overview of example constructs, with specifics provided where applicable.

3.1.2 Communicating with JWS Online via the REST API

A plethora of API methods exist for various websites, but for the sake of simplicity the focus of this discussion will be on the RESTFull web service framework, as this is what is utilised by JWS Online [45].

The REST communications framework allows applications and programs to share information with one another through unified HTTP methods. From a server perspective the REST framework enables the regulation of access to internal application resources, while maintaining open access to services explic-

itly made available by such application endpoints. These service endpoints are accessible to a client in the form of a URL, using the hypertext transfer protocol (HTTP). This ability makes the REST framework specifically suited for a unified communications protocol, as various applications can communicate with one another utilizing the same protocol irrespective of the application in question [45]. Case in point, the availability of the JWS Online API enables the interaction of the Mathematica scripts used here for analysis with the web server, bringing about an expanded use of the JWS Online resources outside of the original project scope.

HTTP requests can be broken down into parts based upon the forward slash character. Consider, as an example, the following url: `http://jjj.biochem.sun.ac.za/rest/models/teusink/mf`. As indicated by the "HTTP://" portion, this request utilizes the hypertext transport protocol (HTTP) of host address jjj.biochem.sun.ac.za. The request is directed at the REST endpoint within the "models" directory to return the "teusink" model in an "mf" format. The result is returned in the form of a nested javascript object notation (JSON) key-value pair , with the model name and content as the first and second entries respectively.

This request can be altered to return models based on specified criteria. For example, metabolic models can be returned by altering the request construct to the following: `http://jjj.biochem.sun.ac.za/rest/models/?id=&organism=&process=1&jwsmodel__model_type=`. In this request, "process=1" refers to models fulfilling the prerequisite of being defined as metabolic processes by annotations added during model creation and curation. A different one of these endpoints in turn enables the incorporation of models from an external resource to within the internal JWS Online database. This proved use-

ful in obtaining additional models, as the BIOMODELS could be integrated as described in section 3.2. For more information on JWS Online specific REST API endpoints, refer to the JWS Online documentation REST section [46].

3.2 Data processing

Data processing consisting of retrieval, sorting and calculations leading to data transformation is discussed in the following section. In alignment with Figure 3.1, the retrieval method (A) will be described first, followed by the data sorting (B) and calculations (C) methods respectively.

3.2.1 Retrieval (A)

With JWS Online providing an endpoint for the retrieval of models from a remote source, as discussed in 3.1.2, the URL handling functions of Mathematica, namely `HTTPRequest` and `URLExecute` were used in the construction of a list of URLs linking to models in JWS Online as well as BIOMODELS repositories. JWS Online presents all current models available as a REST endpoint, whilst BIOMODELS utilises a different API method called SOAP (detailed use instructions are present on the BIOMODELS website). The relevant remote section of the example URL construct

```
http://localhost/rest/fetch/?type={type}&redirect=
{redirect}&remote={remote}
```

can be replaced by the remote model URL. This command, when initiated from the local docker JWS Online instance, fetches and imports a remote model into its internal database. Following this, the model is made available for retrieval in any of the formats supported by JWS Online as a REST endpoint. This raised

the question, which model format would be best suited for the investigation at hand?

An automated algorithm handling metabolic model analysis requires a model format that is generic enough to facilitate the development of unattended automated functions, yet flexible enough to uniformly handle differences among models from various origins, destined for a diverse range of use cases and analyses. As such five key aspects were identified as criteria for a suitable model format.

Firstly, the model format must have a consistent structure, to be able to automate model analyses. The second consideration was the need for a native compatibility with the Mathematica V12 scripting platform. This would facilitate ease of development, as functions designed by previous researchers (that also form part of the JWS Online simulation back-end) could be reused. A third consideration related to the consistency of models upon format conversion. The final converted model needed to impart all of the information, without loss or alteration, that was stored within the original. The final consideration was that the model format of choice should be directly accessible and usable from a computational perspective. A verbose linguistic format would not serve this purpose as additional parsing functions would need to be developed to utilise this data.

Since SBML provides a standardized structure for biological models, it seemed a logical first choice. However, although SBML meets many of the requirements, it does not meet all. Due to the fact that SBML had no native parsing support in Mathematica at the time of development, the ease of development and accessibility aspects proved problematic. Therefore an internal JWS Online standard, the matrix format (MF) was utilised. In MF, data is organized by content type,

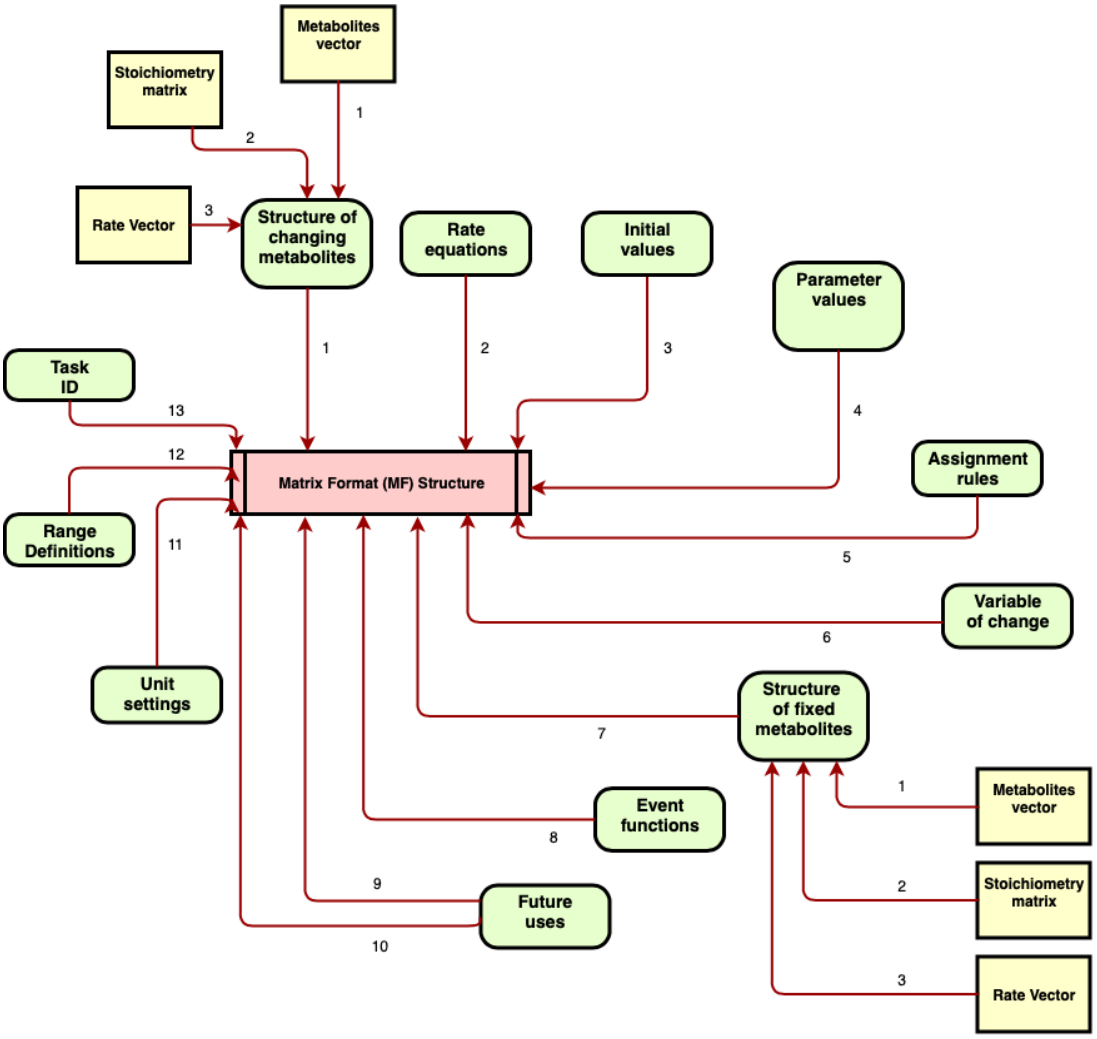

Figure 3.2: A graph representation of the Matrix Format (MF) structure used internally by JWS Online. Within a list context, edge labels represent list element index numbers whereas vertex labels denote content. Colors represent a level shift within the nested list structure.

for example, rate-equations, metabolites, stoichiometry, parameter-sets are all grouped as nested lists, visually illustrated in Figure 3.2, which are directly accessible by Mathematica functions for manipulation and computation. The translation process to matrix format was achieved through the use of the local JWS Online docker installation, whereby a SBML model was retrieved from a

remote server (as described above), and retrieved in matrix format (MF). This format had the added advantage of enabling metabolic control calculations as discussed in Section 3.2.3 to be done via integrated JWS Online functionality. Once a model has been retreived by JWS Online, the end product of the translation process is made available as a REST endpoint allowing for the retrieval of the model. For example, on a public instance of JWS Online the matrix format of the Teusink model can be found at

`https://jjj.bio.vu.nl/rest/models/teusink/mf/`

3.2.2 Sorting (B)

Once all available models have been retrieved and stored within the local repository, the mf versions were retrieved using a REST call to the local server as explained in Section 3.2.1. These models then underwent a sorting process, label B in Figure 3.1, to identify models that do not meet requirements for analyses that follow.

The process starts by exporting the model name to a log file for tracking purpose. At each subsequent sorting step, log files were created, containing model names that satisfy the specific conditions required for further calculations. Model exceptions were captured recorded for graph visualization of the sorting process as shown in Figure 4.1. Here, depending on the sorting step, vertices indicate models or reactions. Edges indicate relationships and direction of procedural flow.

The sorting logic and flow can be seen in the the green block of Figure 3.1. Once a model is retrieved it is sent to function (4.). This function examines the structure of models to identify suitable models for further analysis. The first process evaluates whether or not a model contains any event function. This is done by

extracting the eighth element in the mf of the model (5.). As no apriori knowledge of the timing or effect of these event triggers upon the steady state and control behaviour were available, these models are discarded. A model which passes is then checked for the presence of stoichiometry (6.), done by extracting the stoichiometry in the first position of the model mf list. If the model contains no stoichiometry, it is logged as such and discarded. Model event triggers, of the kind described above, can also be specified in terms of conditional piecewise functions (7.). This identification is done based on testing whether a reaction contains the string term "Piecewise" as this is how the function is specified in mf format.

These steps serve as an initial minimal validation of the suitability of models. The order of operation proved important towards computational efficiency, as these procedures were not as computationally intensive as simulation and calculation operations which follow.

After the structural tests described above, the stability of a model is assessed to ensure the presence of a steady state. For this purpose the stability of a steady state solution is determined by calculating its Jacobian matrix (8.). As is known from linear algebra, the eigenvalues of a Jacobian matrix holds information on the stability of a system of ODE's. The system converges to a stable state if the real parts of eigenvalues are negative, pointing to a decay of perturbations. In contrast, positive eigenvalues point to a divergence from a stable state, as a perturbation is amplified. A third condition, the occurrence of a positive eigenvalue with a non zero imaginary part, is indicative of a system displaying oscillations, be it stable or unstable periodic behaviour [47, 48]. Models exhibiting instabilities were deemed unsuitable for the current analysis and are discarded. For a simple test of stability, a Jacobian matrix that is invertible could also serve

as a positive confirmation of a steady-state [39].

A model that has reached this point in the algorithm is written to a text file for repeated use. Next the model is sent for simulation and calculation procedures as described in the following section and as can be seen in Figure 3.1.

3.2.3 Calculations (C)

Biological model analysis platforms range from stand-alone applications, the likes of Jarnac, COPASI, CellDesigner and BioNetGen, to add-on modules and libraries such as LibRoadRunner, COBRA, Pysces, Scrumpy, SimBiology and Simulink, for the Python and Matlab scripting environments respectively [49–54]. JWS Online utilizes custom Mathematica packages to perform model analysis, as described by [34, 46]. The following section is dedicated to the explanation of individual simulation/calculation steps, leading to the entirety of the automated model analysis algorithm used to generate data forfurther analysis, as described in section 3.3.

The steady-state of a model was calculated and the flux control coefficients were determined using the very same Mathematica packages employed by JWS Online. The functions involve linear algebra methods as described by Hofmeyr[39].

With control coefficients calculated, an additional selection criteria is enforced as a negative own flux control value was deemed improbable, i.e. an increase in enzyme concentration should not lead to a decrease in reaction rate. No further investigation into this was conducted as it lies outside the scope of this thesis.

With regards to disequilibrium ratio calculations, these can only be performed for reactions specified in a reversible manner, refer to section 2.2.1. As such, a

test function was developed to identify these reactions. A reversible reaction is defined as a rate equation containing a negative part within the numerator portion:

$$v_{net} = v_{forward} - v_{reverse} \tag{3.1}$$

thus allowing a rate to become negative (reversed) under certain conditions. Rate equations are therefor separated into numerator and denominator portions. The numerator is recast into base components and tested for the presence of a "-1" term. This is achieved by utilizing the tree form structures available to Mathematica which leads to the equation being expanded to smallest component parts or terms. The indices of these reversible reactions are then stored, on a per model basis, in an intermediate variable for use in disequilibrium calculations later.

From the calculations of flux control coefficients, referred to in section 2.3.3, an inverse of the Jacobian matrix is calculated. If the Jacobian matrix contains very small values, an inverse can approach infinity. This introduced errors due to precision and accuracy limitations of numerical calculations. As such a further step in ensuring model simulation stability was implemented by way of elasticity calculation checks. The largest elasticity value of the system is compared to a threshold chosen as 1×10^{-10}. The choice of this threshold was based on observation of failed calculations from models in a "trial and error manner" whereby at smaller elasticity coefficients, errors in machine precision and accuracy were observed. Models that have sufficiently large elasticities are then passed on to the following step.

To calculate disequilibrium ratios, knowledge of metabolite identity (substrate/product) is needed. The relevant metabolites are identified through the

use of the stoichiometric matrix. One can extract products and substrates on the basis of stoichiometry values that are larger or smaller than zero respectively. Once products have been identified the mass action ratio γ is determined by raising each metabolite in a reaction to the power of its corresponding stoichiometry, leading to the first part of symbolic disequilibrium ratio, ρ, construction. Consider a system of n metabolites and d reactions, for the metabolite vector

$$S = \begin{bmatrix} s_1 \\ s_2 \\ s_3 \\ \vdots \\ s_n \end{bmatrix} \tag{3.2}$$

each row is raised to the corresponding column value from

$$N = \begin{bmatrix} x_{11} & x_{12} & x_{13} & \dots & x_{1n} \\ x_{21} & x_{22} & x_{23} & \dots & x_{2n} \\ \vdots & \vdots & \vdots & \ddots & \vdots \\ x_{d1} & x_{d2} & x_{d3} & \dots & x_{dn} \end{bmatrix} \tag{3.3}$$

such that

$$S^N = \begin{bmatrix} s_1^{x_{11}} & s_2^{x_{12}} & s_3^{x_{13}} & \dots & s_n^{x_{1n}} \\ s_1^{x_{21}} & s_2^{x_{22}} & s_3^{x_{23}} & \dots & s_n^{x_{2n}} \\ \vdots & \vdots & \vdots & \ddots & \vdots \\ s_1^{x_{d1}} & s_2^{x_{d2}} & s_3^{x_{d3}} & \dots & s_n^{x_{dn}} \end{bmatrix} \tag{3.4}$$

The product of the n elements in every row gives the mass action ratios of the d

reactions:

$$\gamma = \begin{bmatrix} s_1^{x_{11}} \cdot s_2^{x_{12}} \cdot s_3^{x_{13}} \dots s_n^{x_{1n}} \\ s_1^{x_{21}} \cdot s_2^{x_{22}} \cdot s_3^{x_{23}} \dots s_n^{x_{2n}} \\ \vdots \\ s_1^{x_{d1}} \cdot s_2^{x_{d2}} \cdot s_3^{x_{d3}} \dots s_n^{x_{dn}} \end{bmatrix} \tag{3.5}$$

From the above it can be seen that stoichiometries of zero will result in factors of one. Negative and positive stoichiometries will result in denominators and numerators respectively, giving the mass action ratio γ of a specific reaction.

K_{eq} calculations can be performed by first symbolically solving for a product of a rate equation set to zero, e.g.

$$v = V_m/K_s \cdot (s - p/K_{eq}) = 0 \tag{3.6}$$

$$p_{eq} = K_{eq} \cdot s_{eq} \tag{3.7}$$

This solution is then substituted into the expression of the mass action ratio (i.e. used to evaluate the mass action ratio at equilibrium) to obtain the symbol(s) for the equilibrium constant:

$$\gamma_{eq} = \frac{p_{eq}}{s_{eq}} \tag{3.8}$$

$$= K_{eq} \tag{3.9}$$

The value of K_{eq} was then either directly extracted from a model's parameter set or, if specified in terms of other constants as is the case for the Haldane relation (e.g. $K_{eq} = {}^{V_m \cdot K_p}/_{V_r \cdot K_s}$), calculated from those constants extracted from the parameter set.

The disequilibrium ratio can then be written as

$$\rho = \frac{\gamma}{K_{eq}} = \frac{\frac{p}{s}}{K_{eq}} \tag{3.10}$$

with the value of K_{eq} known and the steady state concentrations of p and s to be determined from the model at steady state. Substituting steady-state values allows for the numerical calculation of the disequilibrium ratio. This was the generic manner in which disequilibrium calculations were determined. From the methods described above, two values were returned per reaction: the flux control coefficient as well as the disequilibrium ratio.

3.3 Analysis and Visualization

Analysis of the results was facilitated by normalization and visualization methods. This was done as it is often difficult to interpret and compare results in table form alone. Especially with large amounts of reactions present, patterns can easily be overlooked.

Disequilibrium ratios larger than one were inverted to map [1,∞) to [1,0).This was done to place all disequilibrium ratios within the same range $(0 - 1)$ with reactions close to 0 being far from equilibrium and those at 1 at equilibrium.

Visualisation was performed using a Gaussian smoothing kernel within a probability density function using the `SmoothingKernel` function native to Mathematica. The Gaussian kernel treats each individual data point as contributing in part to the overall density of the whole data-set. This is done by expanding a data point to a normal distribution in two dimensions, with x and y coordinates representing the respective means. In the case of this investigation, these are the disequilibrium ratio and flux control coefficients respectively. In Mathematica the `BinWidth` parameter can be adjusted to alter the standard deviation (spreading factor) of these distributions for different resolutions. By applying this smoothing function to each point in the data set, one is able to achieve a collection of normal distributions that smoothly blend all points within the graph

space. The probability density function has the inherent property of leaving the area under the curve equal to one. Therefore, a respective range of flux control coefficient and disequilibrium ratio values, represents a part of the unit probability and allows for a range, rather than discrete values to be analysed. When visualised as a two dimensional graph, the underlying distribution of the full data set becomes apparent as can be seen in Figure 4.2, discussed further in 4.

Another step towards interpreting the results involved the use of a machine learning classifier. Within Mathematica the `Predict` function enables one to train prediction models on a subset of the data and then validate said model against the remaining data. After testing various classifier methods natively available to Mathematica, it was found that the most suitable method (chosen as the one generating the smallest standard deviation) for this distribution was a `RandomForest` classification method, for more information refer to Qi [55]. The end result is a model with a standard deviation of 0.296 when comparing predictions to data in the validation set. This collection of predictors are then incorporated into the predictor model function. From these trained models a prediction of the flux control coefficient, based on a disequilibrium ratio, is made. Since the accuracy of such predictions is based on the underlying training data, with a constant standard deviation, a probability distribution of such a prediction can be used to visualise the confidence interval of the predicted value. This can be seen in Figure 4.4 where the mean but not the standard deviation of the predicted value, is reliant upon the disequilibrium ratio in question.

From data processing to transformation and visualisation, the logical ordering of operations followed a data-flow architecture with individual functions serving as static nodes which process data. Within these functions a control-flow architecture is employed, whereby data remains static as functions are iterated

over specific portions of the data. This hybrid data/control flow architecture proved useful in maintaining accuracy, brought about by control-flow, alongside the speed gains achieved from parallel computing of a data flow paradigm.

Chapter 4

Results and Discussion

The retrieval, sorting and analysis methods described in the previous Chapter were used to obtain models from JWS Online and Biomodels, and to identify suitable reactions for further analysis, namely the calculation of reaction disequilibrium ratios and flux control coefficients. In this chapter the results of this process and the interpretation of the findings relating the disequilibrium ration to flux control are presented.

4.1 Function Tracing

Throughout the algorithm a comma separated log file was updated to keep track of model progression throughout as discussed in Chapter 3. This log file was then visualized as a directed graph which can be seen in Figure 4.1. From this graph, one is able to observe the actions of filter functions as described in Chapter 3. The three lettered nodes A, B and C are the three main function outcomes. Node A represents the point of origin for all models, 778 in total. From this node, models radiate outward, towards the next point of filtering.

Nodes one to three checks for the presence of stoichiometry, event triggers and models with piecewise functions. This was done first as calculations of disequilibrium ratios are directly dependent upon the stoichiometry of the reaction involved. Piecewise functions were identified and filtered, indicated by node four, since by definition these functions can have a discontinuous jump within a certain sub-domain which in turn affects the reliability of the obtained steady-state behaviour of the system. Model events and oscillating reactions lead to a similar problem and as such these were filtered as indicated by node four.

Nodes five, six and seven indicate method check tests where division by zero, flux summation and function time-out errors occurred. Node eight identified models containing no reversible reactions, since disequilibrium ratio calculations on irreversible reactions cannot be calculated using our method. Node eight also indicates a switch from models to individual reactions. As such node B indicated models that have passed filtering operations one to eight, 230 models in total. These were denoted as models that are fit for further calculations and interpretation of flux control coefficients and disequilibrium ratios.

The following numbered filtering functions were applied to the subset of 230 models as is indicated by individual reactions radiating outwards, black lines, from B. These functions perform calculations of flux control coefficient and symbolic equation solving. Figure 4.1 details a legend of the visualised data flow as captured in the log file, with further details discussed in Chapter 3. In this study, our interest is focused on the green lines leading from individual reactions towards node C. These represent 1234 reactions, accumulated from 164 models in total.

The inital 778 models in total, node A, were whittled down to 230 by node B. We ended up with 164 models, node C, which is approximately 20% of all ini-

tial models being used in the final analysis. Appendix A details a full comma-separated list of all 164 model names. On JWS Online, lowercase model names are used, and on BioModels uppercase "BIO" prefixes the names. Due to the different ID formats that are used in the two databases there might be some duplication in models. To be as thorough as possible the contents of both databases were used.

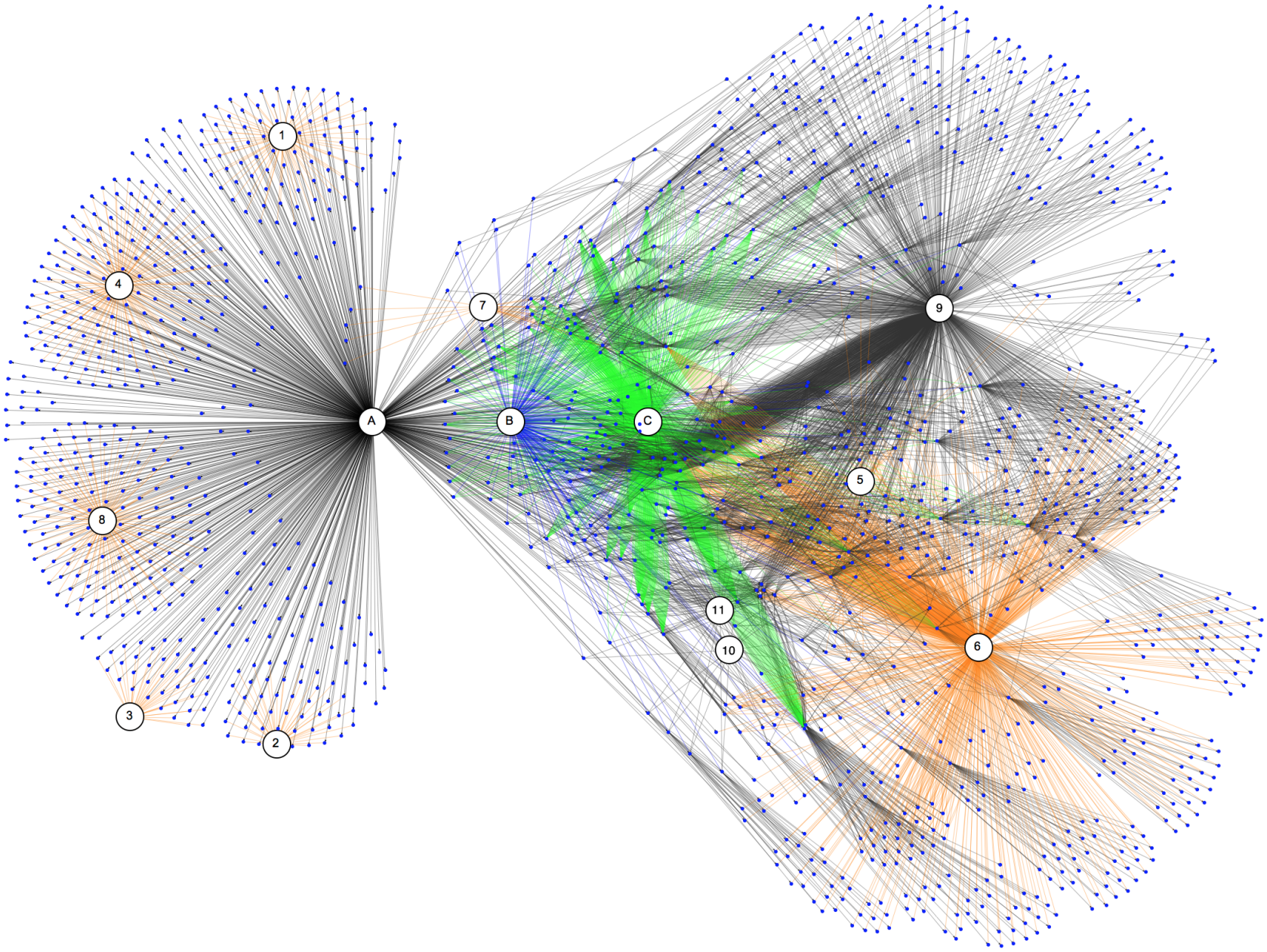

Figure 4.1

Figure 4.1: (Previous page) A directed graph indicating the flow of models as they are handled by the algorithm described in Chapter 3. Important checkpoints are indicated by letters, with A indicating all models at start, 778 at the time of investigation. B denotes models that have been identified as containing reversible rates, 230 models in total, as well as indicating a deviation from model wise investigation towards reaction based calculations. C indicates the final reactions that have passed all check functions, 1234 reactions from 164 models in total. The filtering criteria is labeled by numbers: 1 for no defined stoichiometries, 2 for events, 3 for piecewise functions, 4 for oscillatory behaviour, 5 for division by zero in disequilibrium ratios or control coefficient determinations, 6 for flux summation errors, 7 for simulation time-outs, 8 for no reversible reactions, 9 for no product or substrate, 10 for errors in calculations due to small elasticity coefficients, and 11 for flux calculation errors and no flux results generated at all.

4.2 Disequilibrium ratios and flux control coefficients

Flux control coefficients and disequilibrium ratios were calculated as is discussed in Chapter 3. The control matrix equation approach (eqs 2.33 to 2.35) were used to calculate the control that each reaction has on its own flux. For the disequilibrium ratio the following procedure was followed: first, symbolic equation solving was used to obtain a reaction-appropriate symbolic equilibrium constant and the reaction parameters were substituted from the model specification to obtain a numerical value (similar to eqs 3.7 to 3.9). The mass action ration was determined symbolically using eqs 3.2 - 3.2, and steady state metabolite concentrations from a model simulation were substituted into the appropriate form of eq. 3.10 to obtain the disequilibrium ration.

All results were then mapped to the disequilibrium region of 0 - 1 as to comparably visualize results within the same graph space. A probability density distribution (with a smoothing Gaussian kernel) of the data was then visual-

ized as a contour plot Figure 4.2, from which inferences can be drawn.

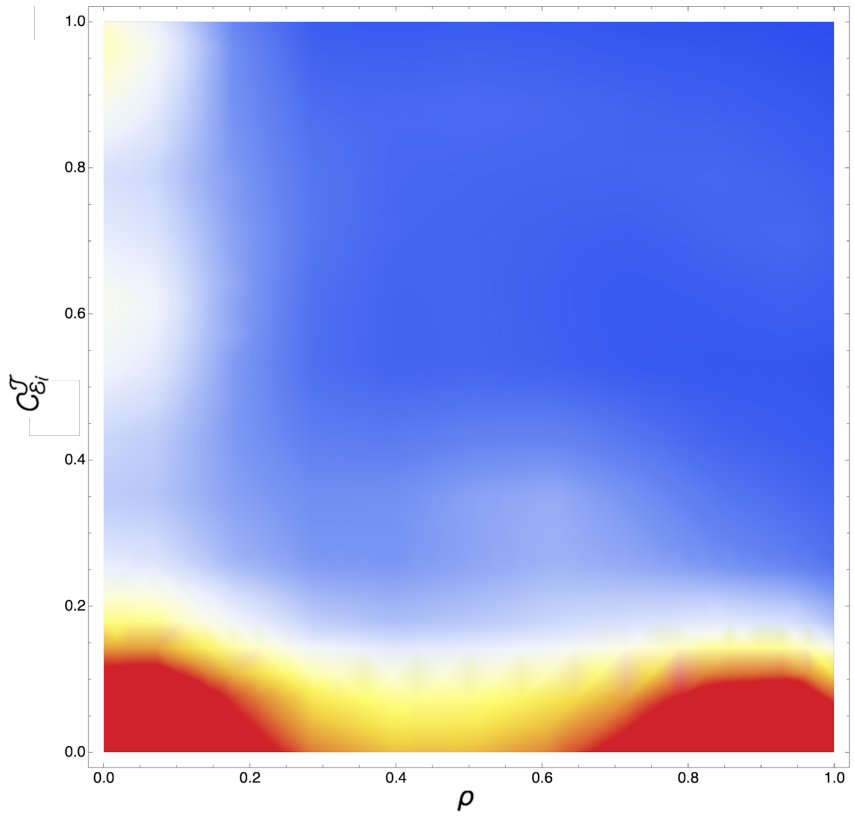

Figure 4.2: Probability density function of flux control coefficients vs disequilibrium ratios (ρ) as outlined in Chapter 3. Red and blue respectively denote higher and lower density of data points relative to the total 1234 data points (reactions).

Upon visual inspection of Fig. 4.2 it is clear that there exists a very strong tendency for reactions with $\rho > 0.2$ to have a small degree of control over their own flux. Clearly there are a large number of data points around the lower left and right regions showing that reactions have a tendency of being either close to equilibrium ($\rho > 0.7$) or far from equilibrium ($\rho < 0.2$) with a marked decrease in number of reactions evident in the $0.2 < \rho < 0.7$ region. This also shows

that most reactions in pathways do not contribute greatly towards the flux control in general. For instance within the Teusink model of glycolysis, discussed in Chapter 3, of 17 reactions only three show flux control coefficient values of larger than 0.2. Within the blue regions we find that there are practically no representative reactions with a control coefficient larger than 0.4 AND $\rho > 0.2$.

Focusing on the $\rho < 0.2$ and $C^J_{v_i} > 0.4$ region a clear tendency is seen for finding a larger than 0.4 control coefficient with many more reactions here than the in entire rest of $\rho > 0.2$ and $C^J_{v_i} > 0.4$ region.

All the reactions included in our analysis have product inhibition via thermodynamic back pressure in the numerator of their rate equations. However, for some reactions (e.g. modelled with mass action kinetics), there is no kinetic product inhibition in the denominator of the reaction rate equation. Figure 4.3 shows the results when a distinction is made between reactions having a product term in the denominator of the rate equation (i.e. kinetic product inhibition) and those without. Here it is evident that reactions without product inhibition, Fig.4.3 (a), tend to lie far from equilibrium and those with, Fig. 4.3 (b), close to equilibrium. However, in both cases the majority of reactions have small flux control coefficients with a comparable fraction having larger control. The effect of product inhibition on flux control has been previously investigated [56, 57] where it was found that including product (or more generally feedback) inhibition in a reaction can lead to a significant shift in the control distribution in a network. The authors argue that realistically one should always include some form of product or feedback effect in reaction equations. In the current study, we have separated out the reactions with no kinetic product inhibition, and noticed a marked difference in ρ values for these reactions compared to the reactions with kinetic inhibition. Due to time constraints, however, we did not

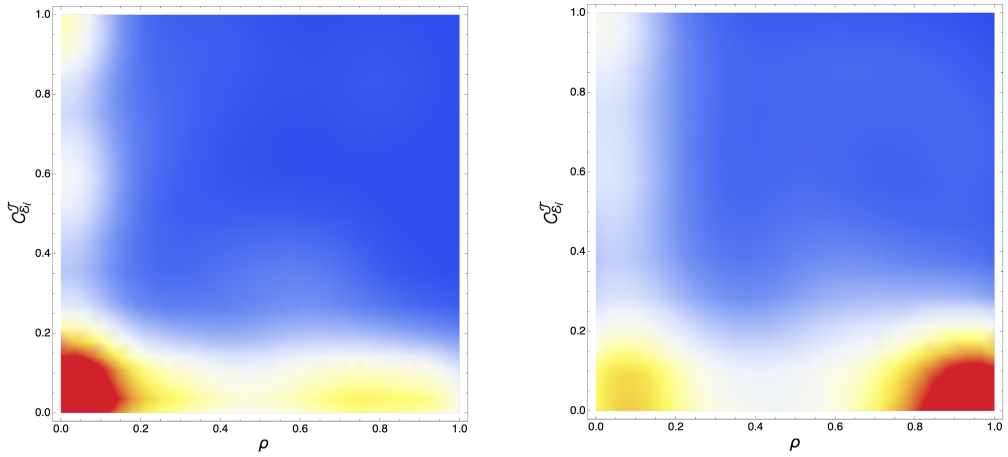

(a) (b)

Figure 4.3: Flux control vs disequilibrium ratio of reactions separated based on kinetic product inhibition. Panel (a) shows results where reversible rate equations did not include a product term in the denominator (779 reactions). Panel (b) is the result of including only reversible rate equations that include a product term in the denominator (473 reactions).

investigate this further and focused on our main aim, namely to investigate the relationship between the mass action ratio and flux control and this was not markedly affected by the presence or absence of the kinetic product inhibition term.

From these results it seems that disequilibrium ratios could indeed reflect the flux control coefficients. Although this might not be in the sense of a sufficiency criterion (if-and-only-if), a very strong tendency is observed for large flux control coefficients to lie in the region of small disequilibrium ratios, $\rho < 0.2$. However a pure visual inspection is lacking in terms of a quantitative description. For confirmation of this observed behaviour, machine learning methods described in Chapter 3 were employed.

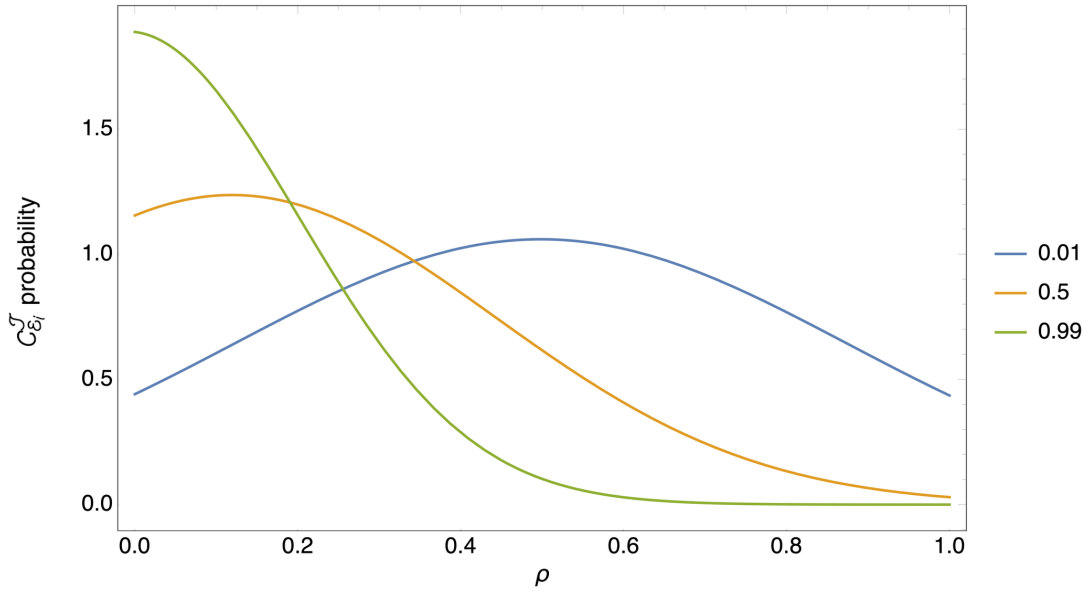

Figure 4.4: Probability density functions of flux control coefficient predictions based on disequilibrium ratios. The Mathematica `Predict` function utilising a `RandomForest` method was used to predict flux control coefficient values of 0.01, 0.5 and 0.99. A flux control coefficient of 0.01 is shown to occur with highest probability at a disequilibrium ratio of 0.5. Similarly a flux control coefficient of 0.99 can be found largely within the $\rho < 0.2$ region.

Machine learning predictors enable a larger quantitative degree of confidence in the visual findings. The disequilibrium ratio and flux control coefficient data was used as training input and output respectively. 20% of the data was utilised in the training of the predictor model and validated against the remainder, as described in Chapter 3, Section 3.3. After training the predictor, the probability density functions of flux control predictions can be calculated. Fig. 4.4 shows the probability (y-axis) of obtaining a flux control coefficient with the value shown in the figure legend, at a given disequilibrium ratio (x-axis). The predictive strength of the disequilibrium ratio is reflected in the width of the distribution of predictions as can be seen in Figure 4.4 with the deviation from

the mean representing the confidence of the trained predictor model.

Flux control coefficient values of $0.01, 0.5$ and 0.99 were chosen to investigate the three regions of interest in the $0 < \rho < 1$ range. In Fig. 4.4 it is evident that reactions in the disequilibrium range of 0.5 to 0.99 have the highest probability of having low flux control coefficients (0.01 is far more probable than 0.5 and 0.99) and the lowest probability of having a high (0.5 to 0.99) flux control coefficient. Conversely, reactions at disequilibrium ratios smaller than 0.5 have the highest probability of having a high (0.5 to 0.99) flux control coefficient. A third condition is observed in Figure 4.4 where reactions contributing small (0.01) flux control coefficients are found across the entire disequilibrium range (the probability of 0.01 is significant across all ρ values). This phenomenon was also observed when constructing Figure 4.2: even though many reactions can be far from equilibrium in a system, it does not necessitate that all reactions far from equilibrium have a large degree of flux control and there are many with very low flux control.

Table 4.1 shows the percentage of reactions that have a disequilibrium ratio smaller than the ρ value of the column with a flux control coefficient larger than the value of the row. This table shows that more than 90% of reactions with significant control (> 0.5) lie in the region $\rho < 0.2$.

Table 4.1: The percentage of reactions that have a disequilibrium ratio smaller than the ρ value of the column with a flux control coefficient larger than the value of the $C^J_{v_i}$ row.

		ρ									
		0.1	0.2	0.3	0.4	0.5	0.6	0.7	0.8	0.9	1.
$C^{\mathcal{J}}_{\varepsilon_i}$	0.	59.8	74.2	74.9	76.1	75.6	78.	81.6	86.5	86.9	89.2
	0.1	66.2	80.5	81.8	83.5	82.7	84.5	86.4	92.2	91.8	91.9
	0.2	69.4	83.2	84.3	85.3	84.4	86.4	88.6	93.	92.3	92.6
	0.3	74.2	89.9	91.2	92.3	92.	93.2	94.1	95.2	94.5	95.3
	0.4	76.9	91.4	91.9	92.8	92.6	93.8	94.5	95.2	94.5	95.3
	0.5	79.5	92.4	92.9	93.8	93.5	94.1	94.9	95.7	95.1	95.9
	0.6	84.5	95.	95.2	96.1	95.7	96.	97.1	97.8	97.8	99.3
	0.7	86.7	96.4	96.5	96.4	96.	96.3	97.1	97.8	97.8	99.3
	0.8	90.3	99.4	99.8	99.7	99.7	99.7	100.	100.	100.	100.
	0.9	93.2	100.	100.	100.	100.	100.	100.	100.	100.	100.

Chapter 5

Conclusion

In this thesis the relationship between disequilibrium ratio and flux control is tested using published enzyme kinetic models. In Chapter 2 it was shown that as reactions occur further away from equilibrium, the predominant factors determining reaction rates shift away from enzyme kinetic regulation close to equilibrium, towards thermodynamic regulation far from equilibrium. To test the extent to which disequilibrium determines flux control in networks of reactions, a method was developed to download, simulate and analyse features of biological models from online repositories in an automated, repeatable and algorithmic manner.

It was found that reactions with disequilibrium ratios smaller than 0.2 did have the largest probability to yield a high flux control coefficient (Fig. 4.2 top left, $C^J_{v_i} > 0.4$). Many reactions were found that are far from equilibrium but have low control (Fig. 4.2 bottom left, $C^J_{v_i} < 0.4$) The presence of some reactions in this region is not unexpected since not all reactions that are far from equilibrium will have a large degree of control in a system if there are multiple such reactions. In fact the flux control summation theorem specifically illustrates

how a system containing a single large flux control reaction requires all other reactions to necessarily have low flux control coefficients. Although all reaction analysed here have thermodynamic product inhibition, many of the reactions in this lower left quadrant were shown to be reactions where kinetic product inhibition has not been taken into account (Fig. 4.3) which might not be physiologically realistic [56, 57]. This was not investigated further in the current study, as the primary aim was to test the relation between ρ and flux control, which showed a similar relationship for the total set of reactions as for the reactions with or without product inhibition.

A few reactions with large flux control coefficients close to equilibrium (Fig. 4.2 top right, $C^J_{v_i} > 0.4$, $\rho > 0.8$) were also found, but they barely appeared in the overall probability distribution view. Some of these were investigated and found to be reactions in systems close to equilibrium as a whole. Within this near equilibrium range, certain reactions will maintain the largest degree of flux control. It is worth noting that this is a very small portion, about 2.8% of all reactions close to equilibrium and with flux control coefficients larger than 0.5.

Machine learning allowed for a probabilistic comparison of the mixed results coming from the large number of reactions. As can be seen in Figure 4.4, a marked increase in the probability of observing a reaction with a larger than 0.5 flux control coefficient is seen as the disequilibrium ratio approaches 0.25 from the left. As the disequilibrium ratio increases from 0.25, the likelihood of finding a flux control coefficient larger than 0.5 is sharply reduced. It is also seen that reactions with low (0.01) flux control coefficients are found across the entire disequilibrium range. When comparing various disequilibrium conditions and flux control coefficient ranges (Table 4.1) it can be seen that the vast majority (91.4%) of flux control coefficients larger than 0.4, were within the disequilib-

rium interval between 0 and 0.2.

We therefore conclude that the vast majority of reactions with high flux control coefficients (> 0.2) have a disequilibrium ratio smaller than 0.2. This disequilibrium range is however not sufficient to ensure high control as there are, in fact, reactions far from equilibrium which have little to no flux control. Conversely, reactions close to equilibrium with $C^J_{v_i} > 0.4$ have also been observed. Nonetheless, the overwhelming majority of reactions with a high flux control coefficient are reactions far away from equilibrium, and it would be a good to check the ρ for a reaction before setting out to engineer a reaction step for increased pathway flux. Although the flux control coefficient is the defining entity for a reaction's control, the probability that a reaction has a high control if its ρ is higher than 0.25 is small.

Developments in online data repositories and communications methods, have made it possible to extract information from a large number of published biological models in a manner such as demonstrated in this thesis. The simulation and analysis presented here can be easily repeated as more models are made available on the databases or even extended to test other hypotheses on a large number of models.

As online model repositories grow, more data is made available for analysis. As such an automated model analysis framework, as described in this thesis, would also prove invaluable towards speeding up the search for effective targets of biotechnological or drug development strategies using appropriate methods of model analysis. With slight modifications, further investigations of this sort can be used to identify alternative systemic properties that can aid in even faster identification of predominant controlling reactions of the system under investigation.

Appendices

A.1 Table of Used Models and Results

Model Name	Reaction Name	Disequilibrium Ratio	FluxCC
branch3	v1	0.21525	0.688982
branch3	v2	0.	0.655509
branch3	v3	0.	0.655509
branch5	v1	0.335287	0.546441
branch5	v2	0.567877	0.36339
branch5	v3	0.567877	0.36339
branch5	v4	0.525205	0.36339
branch5	v5	0.525205	0.36339
bruggeman	v11	0.00264427	0.0318717
bruggeman	v12	$1.84484 * 10^{-11}$	0.0482835
bruggeman	v14	$8.85868 * 10^{-11}$	0.504483
bruggeman	v9	0.104104	0.960373
bruggeman2	v1	0.521738	0.0196173
bruggeman2	v2	0.00737732	0.231962
bruggeman2	v3	0.223675	0.0342021
bruggeman2	v4	0.116153	0.714219
bulik2	v0	0.913997	0.177797
bulik2	v1	$4.58968 * 10^{-7}$	1.88952
bulik2	v10	0.884986	0.0095811
bulik2	v11	0.761503	0.0175826
bulik2	v12	0.832502	0.0559832
bulik2	v13	0.920313	$-1.77957 * 10^{-9}$
bulik2	v14	0.0000562192	0.979401
bulik2	v17	0.00788617	0.0198922
bulik2	v18	0.0330655	0.000152892
bulik2	v2	0.990243	0.0000158577
bulik2	v21	0.999573	$1.82792 * 10^{-9}$
bulik2	v22	0.988721	$1.54469 * 10^{-8}$
bulik2	v23	0.50669	$1.41076 * 10^{-6}$
bulik2	v24	0.981057	$2.7362 * 10^{-8}$
bulik2	v26	0.970009	$4.24995 * 10^{-8}$
bulik2	v27	0.999219	0.
bulik2	v28	0.99982	$2.26182 * 10^{-10}$
bulik2	v29	0.999881	0.00011663
bulik2	v3	$1.21062 * 10^{-6}$	0.000673312
bulik2	v4	0.816754	$4.5253 * 10^{-11}$

Model Name	Reaction Name	Disequilibrium Ratio	FluxCC
bulik2	v5	0.998192	0.
bulik2	v7	0.910505	0.102956
bulik2	v8	0.0545995	-0.0929781
bulik3	v0	0.913761	0.000929506
bulik3	v1	$4.55187 * 10^{-7}$	0.428092
bulik3	v10	0.885403	-0.00303602
bulik3	v11	0.762481	-0.00558928
BIOMD0000000013	E10	0.99195	$4.94774 * 10^{-9}$
BIOMD0000000013	E11	0.999979	$6.27381 * 10^{-11}$
BIOMD0000000013	E12	0.999929	$1.83648 * 10^{-7}$
BIOMD0000000013	E14	1.	$2.44982 * 10^{-9}$
BIOMD0000000013	E15	1.	$1.2971 * 10^{-9}$
BIOMD0000000013	E2	0.999999	$5.46998 * 10^{-8}$
BIOMD0000000013	E3	0.00033387	0.0716378
bulik3	v13	0.920105	0.00140248
BIOMD0000000013	E4	0.999981	$1.71276 * 10^{-6}$
BIOMD0000000013	E5	0.999978	$1.89339 * 10^{-6}$
BIOMD0000000013	E7	0.999996	$1.05681 * 10^{-8}$
BIOMD0000000013	E8	1.	$1.4926 * 10^{-9}$
bulik3	v14	0.0000563045	0.99177
bulik3	v17	0.00787067	0.0077117
bulik3	v18	0.0331028	0.000186555
bulik3	v2	0.990201	0.00291522
bulik3	v21	0.999573	0.000082415
bulik3	v22	0.988709	0.00206812
bulik3	v23	0.508784	0.0651342
bulik3	v24	0.981215	0.00127958
bulik3	v25	0.0000324247	0.890495
bulik3	v26	0.970328	0.00205738
bulik3	v27	0.999219	0.
bulik3	v28	0.999819	$2.82504 * 10^{-6}$
bulik3	v29	0.999881	0.000118093
bulik3	v3	$1.22333 * 10^{-6}$	0.224801
bulik3	v4	0.819697	0.0019312
bulik3	v5	0.998205	0.0000186006
bulik3	v8	0.0545995	0.663439
chassagnole2	v1	0.67711	0.280485
chassagnole2	v2	0.600671	0.249551
chassagnole2	v3	0.00048334	0.464976
cronwright	v1	0.0000599953	0.851818
BIOMD0000000380	hxt	0.000976282	0.888437
BIOMD0000000380	pgi	0.778845	0.00290836
BIOMD0000000380	pgm	0.224275	0.433784
dupreez1	vALD	0.59917	0.00299195
dupreez1	vENO	0.243184	0.000777373
dupreez1	vG3PDH	0.00429408	0.702162
dupreez1	vGAPDH	0.0489722	0.0126468
dupreez1	vGLK	0.00141346	0.153611
dupreez1	vPGI	0.344509	0.0129631

Model Name	Reaction Name	Disequilibrium Ratio	FluxCC
dupreez1	vPGK	0.653366	0.00035348
dupreez1	vPGM	0.661161	0.00028624
dupreez1	vPYK	0.0342436	0.000390988
BIOMD0000000430	reaction1	0.990099	$-1.52063 * 10^{-17}$
BIOMD0000000430	reaction10	0.990099	$2.96184 * 10^{-7}$
BIOMD0000000430	reaction16	0.92081	0.0792657
BIOMD0000000430	reaction23	0.915751	0.00292149
BIOMD0000000430	reaction26	0.92081	0.0792446
BIOMD0000000430	reaction3	0.0625	0.0000986394
BIOMD0000000430	reaction5	0.915751	0.025335
BIOMD0000000430	reaction7	0.92081	0.0791923
BIOMD0000000431	reaction1	0.990099	$1.45536 * 10^{-7}$
BIOMD0000000431	reaction10	0.990099	$8.7579 * 10^{-6}$
BIOMD0000000431	reaction16	0.666667	0.334873
BIOMD0000000431	reaction18	0.292197	0.00154729
BIOMD0000000431	reaction23	0.915751	0.0264817
BIOMD0000000431	reaction24	0.0893146	0.281188
BIOMD0000000431	reaction26	0.666667	0.334408
BIOMD0000000431	reaction28	0.292197	0.00219647
BIOMD0000000431	reaction3	0.0625	0.000283024
BIOMD0000000431	reaction5	0.915751	0.037891
BIOMD0000000431	reaction7	0.666667	0.333358
BIOMD0000000431	reaction9	0.052153	0.00028614
BIOMD0000000204	J4	0.00019996	0.579625
BIOMD0000000218	ACN	0.000922168	0.243372
BIOMD0000000218	CS	$3.72191 * 10^{-6}$	0.755558
BIOMD0000000218	FUM	0.275919	$4.31855 * 10^{-6}$
BIOMD0000000218	ICD1	0.0045952	0.350789
BIOMD0000000218	ICD2	0.0045952	0.656805
BIOMD0000000218	ICL1	0.00022985	0.993513
BIOMD0000000218	ICL2	0.0000206072	0.999401
BIOMD0000000218	KGD	0.00372462	0.000173384
BIOMD0000000218	MDH	0.560427	0.0000215367
BIOMD0000000218	MS	0.0000246646	0.00030135
BIOMD0000000218	SDH	0.00166006	0.00183255
BIOMD0000000218	SSADH	0.0508967	$2.13734 * 10^{-6}$
BIOMD0000000219	ACN	0.00089841	0.243379
BIOMD0000000219	CS	$3.72162 * 10^{-6}$	0.755603
BIOMD0000000219	FUM	0.275906	$4.1975 * 10^{-6}$
BIOMD0000000219	ICD1	0.000745901	0.348072
BIOMD0000000219	ICD2	0.000745901	0.659357
BIOMD0000000219	ICL1	0.000229948	0.993757
BIOMD0000000219	ICL2	0.000020616	0.999427
BIOMD0000000219	KDH	0.0352588	0.152076
BIOMD0000000219	KGD	0.00436174	0.805053
BIOMD0000000219	MDH	0.560452	0.0000209946
BIOMD0000000219	MS	0.0000253148	0.000299111
BIOMD0000000219	ScAS	0.00136048	0.0394514
BIOMD0000000219	SDH	0.00165954	0.00178168

Model Name	Reaction Name	Disequilibrium Ratio	FluxCC
BIOMD0000000219	SSADH	0.274941	0.0034519
BIOMD0000000217	vazglndem	$1.88898 * 10^{-11}$	0.450639
BIOMD0000000217	vazgludem	$1.34544 * 10^{-11}$	0.644496
BIOMD0000000217	vgdh	0.104104	0.960373
BIOMD0000000217	vglndem	$8.85868 * 10^{-11}$	0.504483
BIOMD0000000217	vgludem	$1.84484 * 10^{-11}$	0.0482835
BIOMD0000000217	vgs	0.00264427	0.0318717
BIOMD0000000456	v1	0.00309639	0.228257
BIOMD0000000456	v2	0.0181687	0.768035
BIOMD0000000456	v3	0.	0.169756
BIOMD0000000456	v4	0.	0.833951
BIOMD0000000028	reaction003	0.993049	0.00129054
BIOMD0000000028	reaction007	0.689655	0.446254
BIOMD0000000028	reaction009	0.915751	0.00213343
BIOMD0000000028	reaction0011	0.641802	-0.0519508
BIOMD0000000028	reaction0013	0.666667	0.0289773
BIOMD0000000028	reaction0017	0.680272	0.0256985
BIOMD0000000023	v6	0.000226397	0.427262
BIOMD0000000023	v8	0.104413	0.430496
BIOMD0000000030	reaction003	0.0625	0.000935947
BIOMD0000000030	reaction007	0.0625	0.00113447
BIOMD0000000030	reaction009	0.915751	0.042826
BIOMD0000000030	reaction0011	0.0029091	0.0413613
BIOMD0000000030	reaction0013	0.666667	0.333756
BIOMD0000000030	reaction0017	0.680272	0.320225
BIOMD0000000030	reaction0020	0.915751	0.0428422
BIOMD0000000030	reaction0022	0.00290922	0.0413613
dupreez5	vACEt	0.999597	0.0163991
dupreez5	vALD	0.722196	0.00332157
dupreez5	vENO	0.136849	0.000508113
dupreez5	vG3PDH	0.0000922668	0.889341
dupreez5	vGAPDH	0.104293	0.00961015
dupreez5	vGLK	0.0221479	0.0218833
dupreez5	vGLT	0.0017375	0.895342
dupreez5	vPGI	0.740749	0.000929401
dupreez5	vPGK	0.547055	0.000535895
dupreez5	vPGM	0.554529	0.000343101
dupreez5	vPYK	0.0405271	0.0000930349
BIOMD0000000454	v1	0.00309639	0.228257
BIOMD0000000454	v2	0.0181687	0.768035
BIOMD0000000454	v3	0.	0.169756
BIOMD0000000454	v4	0.	0.833951
BIOMD0000000212	Vasadh	0.717035	0.00791436
BIOMD0000000213	VMTCH	0.266415	0.33187
BIOMD0000000213	VMTD	0.955671	0.0198957
BIOMD0000000213	VNE	0.0124163	0.787307
BIOMD0000000213	VSHMT	0.151884	0.526565
BIOMD0000000102	v1	0.763579	0.190824
BIOMD0000000102	v10	0.61668	0.875614

Model Name	Reaction Name	Disequilibrium Ratio	FluxCC
BIOMD0000000102	v11	0.499762	0.571863
BIOMD0000000102	v12	0.500778	0.862594
BIOMD0000000102	v13	0.99623	0.015065
BIOMD0000000102	v14	0.999969	0.0150641
BIOMD0000000102	v15	0.5	0.0202128
BIOMD0000000102	v8	0.997941	0.00874583
BIOMD0000000102	v9	0.472666	0.613682
feedbackmoi	v1	0.000483942	0.426095
feedbackmoi	v2	0.0238872	0.814693
feedbackmoi	v3	0.0438815	-0.407648
goodman	v1	0.994119	0.00588102
goodman	v3	0.754944	0.139851
goodman	v6	0.83129	0.179382
hoefnagel1	v10	0.300836	0.193328
hoefnagel1	v11	0.012523	0.0979805
hoefnagel1	v13	0.576638	0.315647
hoefnagel1	v14	0.0305659	0.580474
hoefnagel1	v2	0.00066833	0.0184828
hoefnagel1	v5	$1.26391 * 10^{-16}$	1.00032
hoefnagel1	v9	0.896945	0.1469
hoefnagel2	v10	0.836795	0.0239158
hoefnagel2	v11	0.0516743	0.437665
hoefnagel2	v12	0.671096	0.0446609
hoefnagel2	v13	0.814705	0.0225579
hoefnagel2	v14	0.000302322	0.0359272
hoefnagel2	v15	$1.20715 * 10^{-9}$	1.00005
hoefnagel2	v16	$5.22177 * 10^{-8}$	-0.000731829
hoefnagel2	v19	0.	0.0739229
hoefnagel2	v21	0.748342	0.00144622
hoefnagel2	v23	$5.15058 * 10^{-7}$	0.949614
hoefnagel2	v24	0.307662	0.682537
hoefnagel2	v25	0.	0.304267
hoefnagel2	v26	0.000015154	0.0759186
hoefnagel2	v28	0.767026	0.0989425
hoefnagel2	v4	0.749066	-0.0130963
hoefnagel2	v8	0.659985	0.0272726
hoefnagel2	v9	0.98932	0.000723534
hoefnagel-mixedacid	v3	0.274311	0.790526
hoefnagel-mixedacid	v5	0.324671	0.115311
hoefnagel-mixedacid	v6	0.015598	0.062971
hoefnagel-mixedacid	v7	0.000536072	0.0232949
hoefnagel-mixedacid	v8	0.847044	0.178836
kholodenko	v10	0.997318	0.292536
kholodenko	v11	0.994665	0.584806
kholodenko	v15	0.481822	0.133827
kholodenko	v17	0.610355	0.679835
kholodenko	v18	0.796283	0.253398
kholodenko	v19	0.846971	0.846568
kholodenko	v20	0.629107	0.338514

Model Name	Reaction Name	Disequilibrium Ratio	FluxCC
kholodenko	v21	0.991372	0.018216
kholodenko	v22	0.999398	0.0135171
kholodenko	v23	0.995281	0.0130294
kholodenko	v24	0.513522	0.734398
kholodenko	v3	0.00118986	0.781467
kholodenko	v5	0.235285	0.00126095
kholodenko	v6	0.349967	0.000524705
kholodenko	v7	0.690431	0.000995838
kholodenko	v9	0.999043	0.104223
kintuta	v1	0.4	0.133333
kintuta	v2	0.0625	0.733333
kintuta	v3	0.4	0.133333
kintutb	v1	0.55	0.0454545
kintutb	v2	0.181818	0.688312
kintutb	v3	0.1	0.266234
kintutc	v1	0.242308	0.846154
kintutc	v2	0.969231	0.692308
kintutc	v3	0.54127	0.307692
kintutc	v4	0.152493	0.307692
kintutc	v5	0.551587	0.423077
kintutc	v6	0.18705	0.423077
kintutd	v1	0.244493	0.321007
kintutd	v2	0.11689	0.611461
kintutd	v3	0.279929	0.222944
kintutd	v4	0.699822	0.844589
kouril1	v1	$1.00781 * 10^{-6}$	0.828466
kouril1	v2	0.934426	$8.11378 * 10^{-8}$
kouril1	v3	0.953728	$5.41263 * 10^{-8}$
kouril1	v4	0.9272	$8.32319 * 10^{-8}$
kouril1	v5	0.0275938	$1.29145 * 10^{-6}$
kouril2	v1	0.	0.999999
kouril2	v3	0.28559	0.35862
lambeth	v1	-0.0725448	0.283562
lambeth	v10	0.528981	0.13494
lambeth	v11	0.00178394	0.170926
lambeth	v12	0.00222771	0.0070864
lambeth	v2	0.200795	0.0639267
lambeth	v3	0.917826	0.00607652
BIOMD0000000038	v1	0.990273	0.000189264
BIOMD0000000038	v10	0.0000265362	0.273363
BIOMD0000000038	v2	0.956343	0.00227362
BIOMD0000000038	v5	0.965737	0.000189685
BIOMD0000000038	v6	0.822605	0.0136044
BIOMD0000000038	v9	0.0749681	0.0126624
BIOMD0000000041	MiCK	$3.32508 * 10^{-8}$	0.656776
BIOMD0000000041	PCrdiffusion	0.447505	0.154122
BIOMD0000000041	Pidiffusion	0.995563	$4.52468 * 10^{-7}$
BIOMD0000000284	R1	0.220992	0.117942
BIOMD0000000284	R2	0.10497	0.253201

Model Name	Reaction Name	Disequilibrium Ratio	FluxCC
BIOMD0000000284	R3	0.0723724	0.680827
BIOMD0000000284	R4	0.262078	0.0773321
BIOMD0000000284	R5	0.454554	0.0523953
BIOMD0000000284	R6	0.0598714	0.712463
BIOMD0000000284	R7	0.190802	0.0742845
BIOMD0000000284	R8	0.37736	0.0315551
legewie1	v1	0.763579	0.190824
legewie1	v10	0.61668	0.875614
legewie1	v11	0.499762	0.571863
legewie1	v12	0.500778	0.862594
legewie1	v13	0.99623	0.015065
legewie1	v14	0.999969	0.0150641
legewie1	v15	0.5	0.0202128
legewie1	v8	0.997941	0.00874583
legewie1	v9	0.472666	0.613682
leroux	v1	0.0010407	0.741163
leroux	v10	0.999968	0.000262478
leroux	v11	0.923252	0.312896
leroux	v12	0.998879	0.00614918
leroux	v14	$2.86313 * 10^{-12}$	0.105402
leroux	v15	0.	0.0242309
leroux	v2	0.9944	0.894553
leroux	v21	0.999846	0.00188481
leroux	v24	0.999681	0.00387522
leroux	v26	0.99393	0.101774
leroux	v28	0.0143847	0.108995
leroux	v29	0.342125	0.00107449
leroux	v3	0.00114815	0.441311
leroux	v4	0.911519	0.376259
leroux	v5	0.999624	0.00501567
leroux	v7	0.912198	0.614364
leroux	v8	0.00113441	0.839851
leroux	v9	0.922247	0.685491
leroux2	v1	0.000944138	0.807008
leroux2	v10	0.999962	0.000263611
leroux2	v11	0.909261	0.312881
leroux2	v12	0.999068	0.00397363
leroux2	v14	$2.86313 * 10^{-12}$	0.178378
leroux2	v15	0.	0.0410074
leroux2	v2	0.925016	0.0000573326
leroux2	v3	0.000927766	0.583406
leroux2	v4	0.941339	0.665147
leroux2	v5	0.999484	0.00234696
leroux2	v7	0.941732	0.330045
leroux2	v8	0.000960897	0.610585
leroux2	v9	0.908448	0.685483
lin3	v1	0.540042	0.333333
lin3	v2	0.409459	0.333333
lin3	v3	0.	0.333333

Model Name	Reaction Name	Disequilibrium Ratio	FluxCC
lin3moi	v1	0.423009	0.344006
lin3moi	v2	0.791194	0.0834275
lin3moi	v3	0.	0.572566
martins	v1	0.988366	0.00657057
martins	v2	0.151765	0.475414
martins	v3	0.	0.518016
olah	v1	0.0000117938	0.996186
olah	v11	0.581403	$-1.19638 * 10^{-8}$
olah	v2	0.939614	0.00035769
olah	v3	$9.86291 * 10^{-6}$	0.00363802
olah	v4	0.343541	-0.0000470144
olah	v5	0.900149	$-4.74922 * 10^{-6}$
olah	v6	0.000182409	-0.0000751415
olah	v7	0.956351	0.00177811
olah	v8	0.901044	0.00406383
olah	v9	0.446402	0.0237927
poolman	v11	0.995791	$1.67923 * 10^{-9}$
poolman	v12	0.999962	$5.39437 * 10^{-8}$
poolman	v13	0.999989	$2.54594 * 10^{-11}$
poolman	v16	1.	$1.2301 * 10^{-8}$
poolman	v17	0.000231112	0.0300711
poolman	v3	1.	$-1.64445 * 10^{-10}$
poolman	v4	1.	$-1.08175 * 10^{-10}$
poolman	v6	0.999987	$4.02234 * 10^{-7}$
poolman	v7	0.999991	$5.64678 * 10^{-7}$
poolman	v8	0.999998	$3.03504 * 10^{-9}$
poolman	v9	1.	$3.80298 * 10^{-10}$
rohwer1	v6	0.000226397	0.427262
rohwer1	v8	0.104413	0.430496
rohwer2	v1	0.990273	0.000189264
rohwer2	v10	0.0000265362	0.273363
rohwer2	v2	0.956343	0.00227362
rohwer2	v5	0.965737	0.000189685
rohwer2	v6	0.822605	0.0136044
rohwer2	v9	0.0749681	0.0126624
saavedra	v1	0.000187411	1.02785
saavedra	v11	0.0628597	0.553336
saavedra	v12	0.0100622	0.0600195
saavedra	v13	0.00243552	0.00101622
saavedra	v14	0.0189637	0.00143178
saavedra	v4	0.735151	0.0698384
saavedra	v5	0.570473	0.117085
saavedra	v6	0.305913	0.152126
saavedra	v7	0.985584	0.0022996
saavedra	v8	0.813477	0.0650039
saavedra	v9	0.919795	0.0238051
smallbone1	ADH	0.407172	0.0634059
smallbone1	ENO	0.069548	0.0186139
smallbone1	FBA	0.164581	0.382413

Model Name	Reaction Name	Disequilibrium Ratio	FluxCC
smallbone1	glycerolb	0.000935293	0.610564
smallbone1	GPM	0.745199	0.00284735
smallbone1	HXK	0.0107149	0.484198
smallbone1	HXT	0.0167291	0.0804876
BIOMD0000000176	ADH	0.339355	0.0553636
BIOMD0000000176	ENO	0.0747227	0.019268
BIOMD0000000176	FBA	0.111024	0.00924788
BIOMD0000000176	G3PDH	0.000623403	0.548844
BIOMD0000000176	GPM	0.758339	0.00187468
BIOMD0000000176	HXK	0.00666429	0.137489
BIOMD0000000176	HXT	0.00192875	0.933078
BIOMD0000000176	PGI	0.804636	0.00139618
BIOMD0000000176	PGK	0.736318	0.00218958
BIOMD0000000176	PYK	0.00867333	0.00292798
BIOMD0000000176	TDH	0.167734	0.0317983
BIOMD0000000176	TPI	0.999866	$8.75574 * 10^{-6}$
BIOMD0000000294	r13	-1.6995	1.03462
BIOMD0000000294	r14	-1.6995	0.709516
BIOMD0000000294	r15	-0.24495	0.166307
BIOMD0000000294	r18	-0.58841	0.194827
BIOMD0000000294	r19	-0.210191	0.140106
BIOMD0000000172	ADH	0.5018	0.0574448
BIOMD0000000172	ALD	0.203408	0.000590913
BIOMD0000000172	ENO	0.0984735	0.00357732
BIOMD0000000172	G3PDH	0.00152888	0.551572
BIOMD0000000172	GAPDH	0.0431212	0.0842163
BIOMD0000000172	HK	0.00232774	0.21398
BIOMD0000000172	HXT	0.0413667	1.01425
BIOMD0000000172	PGI	0.67752	0.000561355
BIOMD0000000172	PGK	0.563559	0.00191787
BIOMD0000000172	PGM	0.741658	0.00080035
BIOMD0000000172	PYK	0.00626947	0.000526214
BIOMD0000000172	TPI	0.999826	0.0000276491
BIOMD0000000177	ADH	0.395107	0.14617
BIOMD0000000177	ENO	0.0785564	0.0169002
BIOMD0000000177	FBA	0.175924	0.00443689
BIOMD0000000177	G3PDH	0.00066556	0.400284
BIOMD0000000177	HXK	0.00159115	1.05872
BIOMD0000000177	HXT	0.00599315	1.18227
BIOMD0000000177	PGI	0.726277	0.00198757
BIOMD0000000177	PGK	0.543543	0.00658982
BIOMD0000000177	PGM	0.745999	0.00276908
BIOMD0000000177	PYK	0.00441683	0.00215198
BIOMD0000000177	PYRshut	0.254936	0.707636
BIOMD0000000177	TDH	0.0655627	0.178957
BIOMD0000000177	TPI	0.999899	0.0000246478
BIOMD0000000069	v1	0.704285	0.347742
BIOMD0000000197	cellBSPbind	0.000857442	0.989404
BIOMD0000000076	Gpdp	0.0000599953	0.851818

Model Name	Reaction Name	Disequilibrium Ratio	FluxCC
BIOMD0000000191	Argtransp	-4.6957	0.366429
BIOMD0000000071	vGAPdh	0.00165945	0.0682944
BIOMD0000000071	vGlcTr	0.416059	0.888934
BIOMD0000000071	vPGI	0.451572	0.000641526
BIOMD0000000221	ACN	0.0236083	0.0298876
BIOMD0000000221	CS	$3.30956 * 10^{-7}$	0.961608
BIOMD0000000221	FUM	0.883934	0.0000275708
BIOMD0000000221	ICD	0.0000689321	0.707356
BIOMD0000000221	ICL	0.00758853	0.18922
BIOMD0000000221	KDH	0.00328177	0.00506417
BIOMD0000000221	MDH	0.811108	0.000946164
BIOMD0000000221	MS	$2.58513 * 10^{-7}$	0.105007
BIOMD0000000221	ScAS	0.0000658381	0.000555416
BIOMD0000000221	SDH	0.286146	0.000380388
BIOMD0000000222	ACN	0.000226124	0.0945225
BIOMD0000000222	CS	$4.09568 * 10^{-7}$	0.905088
BIOMD0000000222	FUM	0.83666	0.0000156127
BIOMD0000000222	ICD	0.00306484	0.00192754
BIOMD0000000222	ICL	0.0384823	0.889275
BIOMD0000000222	KDH	0.0364258	0.0002487
BIOMD0000000222	MDH	0.895349	0.0000647443
BIOMD0000000222	MS	0.0000104859	0.104841
BIOMD0000000222	ScAS	$9.8241 * 10^{-6}$	0.00323503
BIOMD0000000222	SDH	0.328997	0.000122904
BIOMD0000000115	reaction002	0.509255	0.995182
BIOMD0000000115	reaction004	0.509255	0.00481827
BIOMD0000000116	reaction0	0.215427	0.0251781
BIOMD0000000116	reaction2	0.627185	0.00691339
BIOMD0000000116	reaction4	0.823212	-0.250162
BIOMD0000000116	reaction5	0.931201	-1.16487
achcar1	ALDg	$5.95658 * 10^{-13}$	0.00922999
achcar1	ENOc	0.532343	0.00329203
achcar1	G3PDHg	$8.32619 * 10^{-66}$	0.0200812
achcar1	GDAg	0.277232	0.00023389
achcar1	GKg	0.578496	0.0234697
achcar1	GlcTc	0.0022566	0.911681
achcar1	GlcTg	0.483518	0.000303144
achcar1	GlyTc	0.00159798	0.627281
achcar1	Glytg	0.664075	0.316676
achcar1	HXKg	$1.21554 * 10^{-29}$	0.00953895
achcar1	PFKg	$1.52153 * 10^{-23}$	0.000898463
achcar1	PGA3Tg	0.980035	0.000101788
achcar1	PGAMc	0.1707	0.0211439
achcar1	PGIg	0.0043498	0.000211715
achcar1	PGKg	$6.94514 * 10^{-6}$	0.0023491
achcar1	PYKc	0.0010703	0.00239315
achcar1	TPIg	0.0326774	0.00250114
achcar2	ALDg	$5.75637 * 10^{-14}$	0.0033066
achcar2	DHAPtg	0.327324	0.000399136

Model Name	Reaction Name	Disequilibrium Ratio	FluxCC
achcar2	ENOc	0.531514	0.00271114
achcar2	G3PDHg	$4.26819 * 10^{-63}$	0.0123123
achcar2	GKg	0.586676	0.0229559
achcar2	GlcTc	0.00178342	0.943142
achcar2	GlcTg	0.396307	0.000314672
achcar2	Gly3Ptg	0.90093	0.000345208
achcar2	GlyTc	0.00182116	0.629431
achcar2	Glytg	0.664026	0.318042
achcar2	HXKg	$3.72842 * 10^{-31}$	0.00764737
achcar2	PFKg	$7.75864 * 10^{-27}$	0.000668991
achcar2	PGA3Tg	0.980254	0.000082651
achcar2	PGAMc	0.168983	0.017572
achcar2	PGIg	0.00538043	0.000146584
achcar2	PGKg	0.0000603343	0.0016759
achcar2	PYKc	0.00108281	0.0019666
achcar2	TPIg	0.0360227	0.00187081
achcar4	ALDg	$4.63198 * 10^{-14}$	0.00338474
achcar4	DHAPtg	0.332456	0.000315586
achcar4	ENOc	0.531436	0.0026752
achcar4	G3PDHg	$3.18138 * 10^{-63}$	0.0116811
achcar4	GKg	0.589936	0.0227677
achcar4	GlcTc	0.00175154	0.944961
achcar4	GlcTg	0.38949	0.000315351
achcar4	Gly3Ptg	0.900957	0.000325229
achcar4	GlyTc	0.00191868	0.630726
achcar4	Glytg	0.664012	0.318799
achcar4	HXKg	$2.76651 * 10^{-31}$	0.00751414
achcar4	PFKg	$3.53165 * 10^{-27}$	0.00126816
achcar4	PGA3Tg	0.980275	0.0000814468
achcar4	PGAMc	0.168821	0.017354
achcar4	PGIg	0.00553356	0.00023937
achcar4	PGKg	0.0000692763	0.00163807
achcar4	PYKc	0.001084	0.00194013
achcar4	TPIg	0.0363973	0.00164609
achcar5	ALDg	$7.71315 * 10^{-8}$	0.120113
achcar5	DHAPtg	0.152354	0.0049257
achcar5	ENOc	0.603469	0.00573994
achcar5	G3PDHg	$8.40322 * 10^{-57}$	0.192997
achcar5	GKg	0.0187434	0.144828
achcar5	GlcTc	0.0461916	0.00767627
achcar5	GlcTg	0.971548	$1.9051 * 10^{-6}$
achcar5	Gly3Ptg	0.882421	0.00398774
achcar5	GlyTc	0.000118407	0.524968
achcar5	Glytg	0.673502	0.242688
achcar5	HXKg	$2.50556 * 10^{-30}$	0.00406611
achcar5	PFKg	$1.27214 * 10^{-17}$	0.0231894
achcar5	PGA3Tg	0.961563	0.000446189
achcar5	PGAMc	0.313956	0.0216938
achcar5	PGIg	0.0150406	0.0034089
achcar5	PGKg	$3.70088 * 10^{-20}$	0.0116434

Model Name	Reaction Name	Disequilibrium Ratio	FluxCC
achcar5	PYKc	0.000471336	0.00507902
achcar5	TPIg	0.0374224	0.0344168
achcar6	ALDg	0.0000369441	0.0849828
achcar6	DHAPtg	0.16183	0.00549916
achcar6	ENOc	0.600882	0.0139044
achcar6	G3PDHg	$4.53921 * 10^{-57}$	0.21279
achcar6	GKg	0.000474867	0.280494
achcar6	GlcTc	0.0477719	-0.125778
achcar6	GlcTg	0.972654	-0.0000309123
achcar6	Gly3Ptg	0.884206	0.00213846
achcar6	GlyTc	0.000300029	0.466339
achcar6	Glytg	0.66723	0.228252
achcar6	HXKg	$9.39539 * 10^{-33}$	-0.0708962
achcar6	PFKg	$1.18621 * 10^{-32}$	0.0680006
achcar6	PGA3Tg	0.963585	0.00101124
achcar6	PGAMc	0.308131	0.0534263
achcar6	PGIg	0.0241489	0.0054866
achcar6	PGKg	$3.98711 * 10^{-20}$	0.0296109
achcar6	PYKc	0.000468635	0.0122113
achcar6	TPIg	0.0369062	0.0343393
achcar7	ALDg	$2.36652 * 10^{-15}$	0.000909823
achcar7	DHAPtg	0.415428	0.
achcar7	ENOc	0.530796	0.000433439
achcar7	G3PDHg	$2.74442 * 10^{-65}$	0.00137155
achcar7	GKg	0.619215	0.0212895
achcar7	GlcTc	0.00150004	0.984547
achcar7	GlcTg	0.330779	0.000329156
achcar7	Gly3Ptg	0.901176	0.000152575
achcar7	GlyTc	0.00363607	0.648107
achcar7	Glytg	0.66408	0.328516
achcar7	HXKg	$7.3286 * 10^{-32}$	0.00659846
achcar7	PFKg	$7.44991 * 10^{-32}$	0.000758941
achcar7	PGA3Tg	0.980445	0.0000130517
achcar7	PGAMc	0.167494	0.00283178
achcar7	PGIg	0.00881069	0.000134689
achcar7	PGKg	0.000148639	0.000258466
achcar7	PYKc	0.00109383	0.000313818
achcar7	TPIg	0.0423586	0.0000831078
assmus	v1	0.973872	0.00689831
assmus	v10	0.0855005	0.0000131589
assmus	v12	0.756992	0.0053057
assmus	v13	0.238226	0.0155726
assmus	v15	0.970832	0.0479288
assmus	v16	0.804139	-0.0679582
assmus	v17	0.901364	0.000294217
assmus	v18	0.0114269	0.177937
assmus	v23	0.980873	0.000846477
assmus	v24	0.0113297	0.489202
assmus	v25	0.996946	0.000285761
assmus	v27	-0.076764	0.0496634

Model Name	Reaction Name	Disequilibrium Ratio	FluxCC
assmus	v28	0.994974	0.00349441
assmus	v29	0.999913	0.000146767
assmus	v3	0.0166282	0.286846
assmus	v30	0.99975	0.000436016
assmus	v6	0.503238	0.869404
assmus	v8	0.314422	-0.000564045
assmus	v9	0.788605	0.0000857758
bakker	v1	0.416619	0.887301
bakker	v3	0.451721	0.000646864
bakker	v7	0.0016919	0.0685265
bali	v10	0.962799	$1.0187 * 10^{-7}$
bali	v11	0.798956	$5.31042 * 10^{-7}$
bali	v12	0.00434173	$2.02674 * 10^{-6}$
bali	v13	0.999976	$-2.04114 * 10^{-12}$
bali	v2	0.993373	0.000351976
bali	v3	0.0000277003	0.0325604
bali	v4	0.807302	$-2.73041 * 10^{-7}$
bali	v5	0.997933	$-2.83387 * 10^{-9}$
bali	v6	0.984142	$-3.90664 * 10^{-8}$
bali	v7	0.986618	0.0000569465
bali	v8	0.0804574	0.035623
bali	v9	$3.54474 * 10^{-7}$	0.963636
smallbone10	ADH	0.396628	0.00265674
smallbone10	ENO	0.131	0.0387272
smallbone10	FBA	0.444849	0.372566
smallbone10	GPD	0.000103005	0.610674
smallbone10	GPM	0.738663	0.0117292
smallbone10	HXKGLK1	0.0000503049	1.00045
smallbone10	HXKHXK1	0.0000503049	1.0332
smallbone10	HXKHXK2	0.0000503049	1.69851
smallbone10	HXT	0.0680558	0.0842085
BIOMD0000000482	reaction2	0.99942	0.0224723
BIOMD0000000247	vADH	0.671837	0.0219291
BIOMD0000000247	vALD	0.651558	0.0013887
BIOMD0000000247	vENO	0.363021	0.00696247
BIOMD0000000247	vG3PDH	0.000945899	0.466149
BIOMD0000000247	vGAPDH	0.212746	0.0167617
BIOMD0000000247	vGLK	0.0021548	0.0941816
BIOMD0000000247	vGLT	0.00151732	0.908171
BIOMD0000000247	vPGI	0.464791	0.00773898
BIOMD0000000247	vPGM	0.733247	0.00192048
BIOMD0000000247	vPPI	0.998905	0.
BIOMD0000000247	vR5PI	0.993033	0.
BIOMD0000000247	vTPI	0.770299	0.0100252
BIOMD0000000247	vTransald	0.78191	0.
BIOMD0000000247	vTransk1	0.200954	0.
BIOMD0000000247	vTransk2	0.128942	0.
BIOMD0000000017	R11	0.0415616	0.804139
BIOMD0000000017	R2	0.000234775	0.0274797

Model Name	Reaction Name	Disequilibrium Ratio	FluxCC
BIOMD0000000017	R5	0.974302	0.0174319
BIOMD0000000017	R6	0.340931	0.276496
BIOMD0000000017	R7	0.0800508	0.565721
BIOMD0000000017	R8	$6.07978 * 10^{-15}$	0.0991907
smallbone11	ADH	0.38573	0.00258527
smallbone11	ENO	0.131889	0.0405184
smallbone11	FBA	0.45094	0.359915
smallbone11	GPD	0.0000959032	0.619062
smallbone11	GPM	0.739166	0.012195
smallbone11	HXKGLK1	0.0000505358	1.00042
smallbone11	HXKHXK1	0.0000505358	1.03041
smallbone11	HXKHXK2	0.0000505358	1.63081
smallbone11	HXT	0.0669628	0.082578
smallbone12	ADH	0.369969	0.00263079
smallbone12	ENOENO1	0.217162	0.793131
smallbone12	ENOENO2	0.217162	0.229166
smallbone12	FBA	0.452135	0.377066
smallbone12	GPD	0.0000878788	0.626424
smallbone12	GPM	0.653199	0.0133022
smallbone12	HXKGLK1	0.0000509087	1.00046
smallbone12	HXKHXK1	0.0000509087	1.03273
smallbone12	HXKHXK2	0.0000509087	1.67385
smallbone12	HXT	0.0657862	0.0869376
smallbone13	ADH	0.503027	0.00293766
smallbone13	ENOENO1	0.212505	0.788471
smallbone13	ENOENO2	0.212505	0.216159
smallbone13	FBA	0.573988	0.148796
smallbone13	GPD	0.000123554	0.605316
smallbone13	GPM	0.651991	0.00277272
smallbone13	HXKGLK1	0.000100937	1.00009
smallbone13	HXKHXK1	0.000100937	1.00581
smallbone13	HXKHXK2	0.000100937	1.0803
smallbone13	HXT	0.0686856	0.0574793
smallbone15	ADHADH1	0.104247	0.0350126
smallbone15	ENOENO1	0.210019	0.787843
smallbone15	ENOENO2	0.210019	0.216641
smallbone15	FBA	0.57372	0.154274
smallbone15	GPD	0.000130128	0.601408
smallbone15	GPM	0.777049	0.0015086
smallbone15	HXKGLK1	0.0000987585	1.00011
smallbone15	HXKHXK1	0.0000987585	1.00745
smallbone15	HXKHXK2	0.0000987585	1.12001
smallbone15	HXT	0.0702628	0.0576452
smallbone16	ADHADH1	0.118507	0.0396029
smallbone16	ENOENO1	0.805658	0.823326
smallbone16	ENOENO2	0.805658	0.184922
smallbone16	FBA	0.576938	0.147371
smallbone16	GPD	0.000167355	0.575862
smallbone16	GPM	0.963862	0.00148552
smallbone16	HXKGLK1	0.0000961415	1.00016

Model Name	Reaction Name	Disequilibrium Ratio	FluxCC
smallbone16	HXKHXK1	0.0000961415	1.01174
smallbone16	HXKHXK2	0.0000961415	1.22439
smallbone16	HXT	0.0735079	0.0592063
smallbone17	ADHADH1	0.118437	0.0402416
smallbone17	ENOENO1	0.803638	0.823113
smallbone17	ENOENO2	0.803638	0.185136
smallbone17	FBA	0.577933	0.146976
smallbone17	GPD	0.000163815	0.575886
smallbone17	GPM	0.963232	0.0014967
smallbone17	HXKGLK1	0.0000986033	1.00016
smallbone17	HXKHXK1	0.0000986033	1.01184
smallbone17	HXKHXK2	0.0000986033	1.22505
smallbone17	HXT	0.0731769	0.0598336
smallbone18	ADHADH1	0.0353417	0.385486
smallbone18	ENOENO1	0.755011	0.829316
smallbone18	ENOENO2	0.755011	0.187566
smallbone18	FBA	0.555249	0.105701
smallbone18	GPD	0.000112774	0.875773
smallbone18	GPM	0.955811	0.0029024
smallbone18	HXKGLK1	0.000418101	1.00339
smallbone18	HXKHXK1	0.000418101	1.10518
smallbone18	HXKHXK2	0.000418101	1.8867
smallbone18	HXT	0.00857441	1.46701
smallbone2	ADH	0.883795	0.0888264
smallbone2	ENO	0.132712	0.00784747
smallbone2	FBA	0.063763	0.00904659
smallbone2	glycbranch	0.0056655	-0.517752
smallbone2	GPM	0.725084	0.00324933
smallbone2	HXKGLK1	0.0000186149	1.00058
smallbone2	HXKHXK1	0.0000186149	1.08085
smallbone2	HXKHXK2	0.0000186149	3.54955
smallbone2	HXT	0.294585	0.0239618
smallbone3	ADH	0.584329	0.0800371
smallbone3	ENO	0.140266	0.0175517
smallbone3	FBA	0.218609	0.058115
smallbone3	glycbranch	0.00181267	0.441343
smallbone3	GPM	0.74659	0.00467636
smallbone3	HXKGLK1	0.0000486913	1.0008
smallbone3	HXKHXK1	0.0000486913	1.04243
smallbone3	HXKHXK2	0.0000486913	1.80647
smallbone3	HXT	0.051663	0.109896
smallbone4	ADH	0.329178	0.0205665
smallbone4	ENO	0.179573	0.0112904
smallbone4	FBA	0.49531	0.0139803
smallbone4	GPD	0.0000698551	0.64806
smallbone4	GPM	0.761627	0.00274343
smallbone4	HXKGLK1	0.0000627582	1.0002
smallbone4	HXKHXK1	0.0000627582	1.00592
smallbone4	HXKHXK2	0.0000627582	1.07047

Model Name	Reaction Name	Disequilibrium Ratio	FluxCC
smallbone4	HXT	0.0433639	0.0809505
smallbone5	ADH	0.326706	0.0177258
smallbone5	ENO	0.187118	0.00956218
smallbone5	FBA	0.502645	0.0107259
smallbone5	GPD	0.000066279	0.651002
smallbone5	GPM	0.764374	0.00229387
smallbone5	HXKGLK1	0.0000585412	1.00022
smallbone5	HXKHXK1	0.0000585412	1.00607
smallbone5	HXKHXK2	0.0000585412	1.07079
smallbone5	HXT	0.0425625	0.0828406
smallbone6	ADH	0.342867	0.027396
smallbone6	ENO	0.171831	0.0144141
smallbone6	FBA	0.486645	0.0181729
smallbone6	GPD	0.0000781434	0.631521
smallbone6	GPM	0.757591	0.0036511
smallbone6	HXKGLK1	0.0000500337	1.00061
smallbone6	HXKHXK1	0.0000500337	1.02342
smallbone6	HXKHXK2	0.0000500337	1.32756
smallbone6	HXT	0.045396	0.118703
smallbone7	ADH	0.460624	0.000820667
smallbone7	ENO	0.187018	0.00605732
smallbone7	FBA	0.392186	0.0205657
smallbone7	GPD	0.00018725	0.247834
smallbone7	GPM	0.762975	0.00149852
smallbone7	HXKGLK1	0.0000489344	1.00064
smallbone7	HXKHXK1	0.0000489344	1.02247
smallbone7	HXKHXK2	0.0000489344	1.2924
smallbone7	HXT	0.0436628	0.123587
smallbone8	ADH	0.2213	0.000967473
smallbone8	ENO	0.15539	0.0601992
smallbone8	FBA	0.569964	0.0923322
smallbone8	GPD	0.0000324821	0.656155
smallbone8	GPM	0.749977	0.0163386
smallbone8	HXKGLK1	0.0000526894	1.00031
smallbone8	HXKHXK1	0.0000526894	1.01538
smallbone8	HXKHXK2	0.0000526894	1.23878
smallbone8	HXT	0.0525613	0.0878462
smallbone9	ADH	0.335357	0.00207953
smallbone9	ENO	0.137276	0.0457187
smallbone9	FBA	0.577965	0.189231
smallbone9	GPD	0.0000677765	0.637654
smallbone9	GPM	0.74199	0.0133207
smallbone9	HXKGLK1	0.0000514858	1.00034
smallbone9	HXKHXK1	0.0000514858	1.02182
smallbone9	HXKHXK2	0.0000514858	1.41744
smallbone9	HXT	0.0617531	0.0799611
snoep	v1	0.00289804	0.648706
snoep	v3	0.817092	0.0489009
snoep1	v4	0.241463	$8.48946 * 10^{-6}$

Model Name	Reaction Name	Disequilibrium Ratio	FluxCC
snoep2	v2	0.651363	0.000534516
snoep2	v4	0.241463	0.00077366
supplydemand	v1	0.000290303	0.999705
supplydemand	v2	0.215347	0.000227807
supplydemand	v3	0.399898	0.0000670108
supplydemand2	v1	0.0000918231	0.00135594
supplydemand2	v2	0.654006	$3.86405 * 10^{-8}$
supplydemand2	v3	0.862757	$1.11326 * 10^{-8}$
teusink	v1	0.00141828	0.15343
teusink	v10	0.245045	0.00267259
teusink	v14	0.00197487	0.971436
teusink	v15	0.705319	0.0259738
teusink	v16	0.0016305	0.562381
teusink	v2	0.347758	0.00245203
teusink	v6	0.599836	0.000394735
teusink	v7	0.0503189	0.0421458
teusink	v8	0.656238	0.00120165
teusink	v9	0.662088	0.000981416
teusink2	v3	0.114473	0.
twoenzymecompinh1	v1	0.0422426	0.623812
twoenzymeparcomp1	v1H	0.0422426	0.623812
twoenzymeparcomp1	v1P	0.0422426	0.623812
twoenzymeparcomp2	v1H	0.0422426	0.623812
twoenzymeparcomp2	v1P	0.0422426	0.623812
vaneunen1	v1	0.0498951	0.513009
vaneunen1	v10	0.868711	$9.8227 * 10^{-8}$
vaneunen1	v11	0.380987	$5.33171 * 10^{-7}$
vaneunen1	v12	0.241677	$6.81587 * 10^{-7}$
vaneunen1	v16	0.0844382	0.0000227354
vaneunen1	v2	0.0000376481	0.486371
vaneunen1	v4	0.695417	0.000119573
vaneunen1	v7	0.501392	0.0000397635
vaneunen1	v9	0.0035014	0.000122414
vaneunen2	v10	0.888379	$4.04599 * 10^{-8}$
vaneunen2	v11	0.36816	$2.81611 * 10^{-7}$
vaneunen2	v12	0.14933	$5.482 * 10^{-7}$
vaneunen2	v2	0.000214835	0.134665
vaneunen2	v4	0.720611	0.00023384
vaneunen2	v7	0.347107	0.0000275571
vaneunen2	v9	0.00318877	0.0000562865
vaneunen3	v10	0.832179	$1.20171 * 10^{-8}$
vaneunen3	v11	0.319212	$5.41606 * 10^{-8}$
vaneunen3	v12	0.293618	$3.97263 * 10^{-8}$
vaneunen3	v2	0.000133952	0.493038
vaneunen3	v4	0.726836	0.000316791
vaneunen3	v7	0.53394	$8.84142 * 10^{-6}$
vaneunen3	v9	0.000952302	0.0000360891
vaneunen4	v10	0.869072	$3.40359 * 10^{-7}$
vaneunen4	v11	0.229305	$2.84531 * 10^{-6}$

Model Name	Reaction Name	Disequilibrium Ratio	FluxCC
vaneunen4	v12	0.202744	$2.55791 * 10^{-6}$
vaneunen4	v2	0.00122719	0.13177
vaneunen4	v4	0.797414	0.000669516
vaneunen4	v7	0.491854	0.000102626
vaneunen4	v9	0.0038065	0.000339221
vanheerden1	v1	0.0000588597	0.340038
vanheerden1	v10	0.450052	0.00924688
vanheerden1	v14	0.0146835	0.32268
vanheerden1	v2	0.469444	0.0985534
vanheerden1	v6	0.655818	0.0193566
vanheerden1	v8	0.785664	0.00271189
vanheerden1	v9	0.76954	0.00278059
wortel4	v4	0.274988	0.0122401

Bibliography

[1] Khalil, H. S., Mitev, V., Vlaykova, T., Cavicchi, L., and Zhelev, N. Discovery and development of Seliciclib. How systems biology approaches can lead to better drug performance. *J. Biotechnol.*, 202:40–49, 2015.

[2] Boogerd, F. C., Bruggeman, F. J., Hofmeyr, J.-H. S., and Westerhoff, H. V. *Systems Biology (Philosophical Foundations)*. Elsevier, first edition, 2007.

[3] Kell, D. B. Systems biology, metabolic modelling and metabolomics in drug discovery and development. *Drug Discov. Today*, 11(23-24):1085–1092, 2006.

[4] Fell, D. *Understanding the control of metabolism*. Frontiers in Metabolism. Portland Press, London, England, 2004 edition, 1996.

[5] Schneider, E. D. and Kay, J. J. Life as a manifestation of the second law of thermodynamics. *Math. Comput. Model.*, 19(6-8):25–48, 1994.

[6] Kondepudi, D. and Prigogine, I. *Modern Thermodynamics From Heat Engines to Dissipative Structures. 2nd Edition*. Wiley, 2014.

[7] Lebowitz, J. L. Boltzmann ' S Entropy and Time's Arrow. *Phys. Today*, September 1993:32–38, 1994.

[8] Roos, N. Entropic forces in Brownian motion. *Am. J. Phys.*, 82(12):1161–1166, 2014.

[9] Kramers, H. A. Brownian motion in a field of force and the diffusion model of chemical reactions. *Physica*, 7(4):284–304, Apr. 1940.

[10] Burada, P. S., Hänggi, P., Marchesoni, F., Schmid, G., and Talkner, P. Diffusion in confined geometries. *Chemphyschem*, 10(1):45–54, 2009.

[11] Job, G. and Rüffler, R. Entropy and Temperature. *Physical Chemistry from a Different Angle*, pages 49–92, 2016.

[12] Leffler, J. E. The enthalpy-entropy relationship and its implications for organic chemistry. *J. Org. Chem.*, 20(9):1202–1231, 1955.

[13] Teusink, B., Passarge, J., Reijenga, C. a., Esgalhado, E., Van Der Weijden, C. C., Schepper, M., Walsh, M. C., Bakker, B. M., Van Dam, K., Westerhoff, H. V., and Snoep, J. L. Can yeast glycolysis be understood terms of vitro kinetics of the constituent enzymes? Testing biochemistry. *Eur. J. Biochem.*, 267(17):5313–5329, 2000.

[14] Sorribas, A., Curto, R., and Cascante, M. Comparative characterization of the fermentation pathway of Saccharomyces cerevisiae using biochemical systems theory and metabolic control analysis: Model validation and dynamic behavior. *Math. Biosci.*, 130(1):71–84, 1995.

[15] van't Hoff, M. J. H. Etudes de dynamique chimique. *Recueil des Travaux Chimiques des Pays-Bas*, 3(10):333–336, 1884. ISSN 01650513. doi: 10.1002/recl.18840031003. URL http://doi.wiley.com/10.1002/recl.18840031003.

[16] Waage, P. and Gulberg, C. M. Studies concerning affinity. *J. Chem. Educ.*, 63(12): 1044, 1986.

[17] Voit, E. O., Martens, H. A., and Omholt, S. W. 150 Years of the Mass Action Law. *PLoS Comput. Biol.*, 11(1):1–7, 2015.

[18] Planck, M. and Ogg, A. *Treatise on Thermodynamics*. Longmans Green, London, Dec. 1903.

[19] Ferner, R. E. and Aronson, J. K. Cato Guldberg and Peter Waage, the history of the Law of Mass Action, and its relevance to clinical pharmacology. *Br. J. Clin. Pharmacol.*, 81(1):52–55, 2016.

[20] Copeland, R. A. *Enzymes: A Practical Introduction to Structure, Mechanism, and Data Analysis*, volume 44. John Wiley & Sons, Apr. 2000.

[21] Hynne, F., Danø, S., and Sørensen, P. G. Full-scale model of glycolysis in saccharomyces cerevisiae. *Biophys. Chem.*, 94(1-2):121–163, 2001.

[22] Conradie, R. *A comparative analysis of the G1/S transition control in kinetic models of the eukaryotic cell cycle*. PhD thesis, Stellenbosch: University of Stellenbosch, 2009.

[23] Kacser, H. and Burns, J. A. Molecular democracy: who shares the controls? *Biochem. Soc. Trans.*, 7(5):1149–1160, 1979.

[24] Kacser, H. and Burns, J. A. Causality, Complexity and Computers. In *Quantitative Biology of Metabolism*, pages 11–23. Springer Berlin Heidelberg, 1968.

[25] Fell, D. A. Metabolic Control Analysis : a survey of its theoretical and experimental development. *J. Biochem.*, 330:313–330, 1992.

[26] Heinrich, R. and Rapoport, T. A. A Linear Steady-State Treatment of Enzymatic Chains: General Properties, Control and Effector Strength. *Eur. J. Biochem.*, 42(1): 89–95, 1974.

[27] Rapoport, T. A., Jacobasch, G., and Rapoport, S. A Linear Steady-State Treatment of Enzymatic Chains A Mathematical Model of Glycolysis of Human Erythrocytes. *Eur. J. Biochem.*, 120:107–120, 1974.

[28] Kacser, H. and Burns, J. A. The Control of flux. *Symp. Soc. Exp. Biol.*, 27:65–104, 1973.

[29] Kacser, H. and Burns, J. A. The molecular basis of dominance. *Genetics*, 97(3-4): 639–666, 1981.

[30] Holms, H. Flux analysis and control of the central metabolic pathways in escherichia coli. *FEMS Microbiol. Rev.*, 19(2):85–116, 1996.

[31] Cornish-Bowden, A. Biotechnology and Medicine. *Nat. Biotechnol.*, 17:641–643, 1999.

[32] Boren, J., Montoya, A. R., De Atauri, P., Comin-Anduix, B., Cortes, A., Centelles, J. J., Frederiks, W. M., Van Noorden, C. J. F., and Cascante, M. Metabolic control analysis aimed at the ribose synthesis pathways of tumor cells: A new strategy for antitumor drug development. *Mol. Biol. Rep.*, 29(1-2):7–12, 2002.

[33] Cascante, M., Boros, L. G., Comin-anduix, B., Atauri, P. D., Centelles, J. J., and Lee, P. W. Metabolic control analysis in drug discovery and disease. *Nat. Biotechnol.*, 20:243–250, 2002.

[34] Olivier, B. G. and Snoep, J. L. Web-based kinetic modelling using JWS Online. *Bioinformatics*, 20:2143–2144, 2004.

[35] Weselake, R. J., Shah, S., Tang, M., Quant, P. A., Snyder, C. L., Furukawa-Stoffer, T. L., Zhu, W., Taylor, D. C., Zou, J., Kumar, A., Hall, L., Laroche, A., Rakow, G., Raney, P., Moloney, M. M., and Harwood, J. L. Metabolic control analysis is helpful for informed genetic manipulation of oilseed rape (Brassica napus) to increase seed oil content. *J. Exp. Bot.*, 59(13):3543–3549, 2008.

[36] Westerhoff, H. V. and Chen, Y.-d. How do enzyme activities control metabolite concentrations? An additional theorem in the theory of metabolic control. *Eur. J. Biochem.*, 142:425–430, 1984.

[37] Kacser, H., Burns, J. A., and Fell, D. A. The control of flux. *Biochem. Soc. Trans.*, 23 (2):341–366, 1995.

[38] Ehlde, M. and Zacchi, G. A general formalism for Metabolic Control Analysis. *Chem. Eng. Sci.*, 52(15):2599–2606, 1997.

[39] Hofmeyr, J.-H. S. Metabolic control analysis in a nutshell. *Proceedings of the 2nd International Conference on Systems Biology*, ii:291–300, 2001.

[40] Sauro, H. M. Control and regulation of pathways via negative feedback. *J. R. Soc. Interface*, 14(127), 2017.

[41] Rohwer, J. M. and Hofmeyr, J.-H. S. Kinetic and thermodynamic aspects of enzyme control and regulation. *J. Phys. Chem. B*, 114(49):16280–16289, 2010.

[42] Imielinski, T. and Mannila, H. Perspective on Knowledge Discovery. *Commun. ACM*, 39(11):58–64, 1996.

[43] Radivojac, P., Chawla, N. V., Dunker, A. K., and Obradovic, Z. Classification and knowledge discovery in protein databases. *J. Biomed. Inform.*, 37(4):224–239, 2004.

[44] Uppalaiah, B., Chandra, N. S., Gandhi, R. V., and Babu, G. C. A framework for knowledge discovery, knowledge use and knowledge management. *International Journal of Scientific and Engineering Research*, 3(1):1–6, 2012.

[45] Christie, T. Django RESTfull Webservice, Accessed 30 Sept 2020. URL http://www.django-rest-framework.org.

[46] Olivier, B. JWSOnline Documentation, Accessed 30 Sept 2020. URL https://jws-docs.readthedocs.io/8_rest.html.

[47] Wang, L., Birol, I., and Hatzimanikatis, V. Metabolic control analysis under uncertainty: Framework development and case studies. *Biophys. J.*, 87:3750–3763, 2004.

[48] du Preez, F. B. *Comparative cross-species analysis of detailed kinetic models of glycolysis*. PhD thesis, University of Stellenbosch, 2009.

[49] Sauro, H. M. and Fell, D. A. Jarnac: a system for interactive metabolic analysis. In: Animating the Cellular Map. *Proceedings of the 9th International Meeting on BioThermoKinetics*, pages 221–228, 2000.

[50] Hoops, S., Sahle, S., Gauges, R., Lee, C., Pahle, J., Simus, N., Singhal, M., Xu, L., Mendes, P., and Kummer, U. COPASI: a COmplex PAthway SImulator. *Bioinformatics*, 22:3067–3074, 2006.

[51] Olivier, B., Rohwer, J., and Hofmeyr, J.-H. S. Modelling cellular systems with PySCeS. *Bioinformatics*, 21(4):560–561, 2005.

[52] Somogyi, E. T., Bouteiller, J. M., Glazier, J. A., König, M., Medley, J. K., Swat, M. H., and Sauro, H. M. LibRoadRunner: A high performance SBML simulation and analysis library. *Bioinformatics*, 31(20):3315–3321, 2015.

[53] Harris, L. A., Hogg, J. S., Tapia, J. J., Sekar, J. A. P., Gupta, S., Korsunsky, I., Arora, A., Barua, D., Sheehan, R. P., and Faeder, J. R. BioNetGen 2.2: Advances in rule-based modeling. *Bioinformatics*, 32(21):3366–3368, 2016.

[54] Laurent, H., Sylvain, A., Thomas, P., Sebastian, N., and Anne, Richelle, e. a. Creation and analysis of biochemical constraint-based models: the COBRA Toolbox v3.0. *ArXiv e-prints*, 2017.

[55] Qi, Y. Random forest for bioinformatics. In Zhang, C. and Ma, Y., editors, *Ensemble Machine Learning: Methods and Applications*, pages 307–323. Springer US, Boston, MA, 2012.

[56] Fell, D. A. and Sauro, H. M. Metabolic control and its analysis. additional relationships between elasticities and control coefficients. *Eur. J. Biochem.*, 148(3):555–561, 1985.

[57] Cornish-Bowden, A. and Cardenas, M. L. Information transfer in metabolic pathways. *Eur. J. Biochem.*, 268(24):6616–6624, 2001.